Republic of Iraq
Ministry of Higher Education
And Scientific Research
University of Kerbala
College of Science
Department of Physics

Synthesis and Characterization of TiO_2 Nanoparticles by Microwave and its Application toward Water Treatment

A Thesis

Submitted to the College of Science of University of Kerbala in partial fulfillment of the requirements for the degree of Master of Science in Physics

by

Ridha Salah Mohammed Jalawkhan

Supervised by

Assist. Prof. Dr. Firas K. M. Alosfur **Prof. Dr. Ahmed M. Abdul Al-Lateef**

2021 A.D 1442 A.H

بِسْمِ اللَّهِ الرَّحْمَنِ الرَّحِيمِ

﴿ وَعَلَّمَكَ مَا لَمْ تَكُن تَعْلَمُ ۚ
وَكَانَ فَضْلُ اللَّهِ عَلَيْكَ عَظِيماً ﴾

صدق الله العلي العظيم

القرآن الكريم - سورة النساء (113)

الإهداء

لسَيدي الحُسَين بن عَلي بن اَبي طالِب كما يَليقُ بِهِ ..

إنْ لَمْ يَكُ لَكَ.. بِكُلِ ما فيكَ مِن كِبرِياءٍ وَحُبٍ وبَقاء .

فَلِمَن أهدي جُهدَ السنين.. مَشفوعاً بابتِسامَةِ رَجاء.

✍ رضا جلوخان

Acknowledgments

First of all, I am thankful to the Merciful, Omniscient Almighty ***ALLAH*** for the help and blessing always. I would like to express my deep thanks and appreciation to ***Assist. Prof. Dr. Firas K. M. Alosfur*** and ***Prof. Dr. Ahmed M. Abdul Al-Lateef*** for their kind advice, valuable guidance and encouragement during supervision of this work. I would like to thank all those who helped me do this job, in particular my esteemed professors in the Physics Department of College of Science at Kerbala University. Thanks are extended to ***Prof. Dr. Rajaa Abdul Ameer Madlool***, ***Assist. Prof. Dr. Noor J. Ridha*** and ***Assist. Prof. Dr. Ali Jalawkhan*** for their continuous support and grateful care during the period of research. Many thanks with heartiest gratitude and respect to ***my father*** and ***mother*** them have always loved me unconditionally and they good examples have taught me to work hard for the things that I aspire to achieve. ***My brothers***, ***my sister*** and ***my close friends*** especially (**M. Jawad Alshahristani**, **Ali A. Sedki** and **M. Mehdy Majeed**) for their love, continuous support, patience and encouragement throughout the period of my study.

Ridha ✍

Abstract

In this study, titanium dioxide (TiO_2) was synthesized using the microwave method as a rapid, uncostly, and effective method. In order to study the effect of the solvent and the power on the morphology, particle size, and the specific surface area of the prepared samples, two different solvents were used. The first solvent was Ethylene Glycol (EG, 99.8%) and the other was Deionized Water (DIW), while titanium isopropoxide $Ti[OCH(CH_3)_2]_4$ (TTIP) was used as TiO_2 precursor. A commercial microwave oven was used with three different powers and 5 minutes was selected as a duration of the preparation time. The prepared specimens were annealed at 400 °C for 1 h.

In present work, diverse techniques were used to study the structure and the morphology of the prepared samples, such as X-Ray Diffraction (XRD), Brunaner-Emmett-Teller (BET) technique, Field Emission Scanning Electron Microscopy coupled with Energy-Dispersive X-ray spectroscopy (FESEM-EDX), and Fourier Transforms Infrared spectroscopy (FTIR). Noticeably, the XRD results revealed that the prepared samples were pure TiO_2 in the anatase phase. The surface area of TiO_2 nanoparticles has been estimated using BET analysis, which indicated that the samples have a large specific surface area and high porosity (for the samples prepared with DIW were higher than samples prepared with EG). The FESEM results showed that the prepared TiO_2 samples were nanorods-like shape when EG was used as a solvent. In contrast, spherical agglomerated nanoparticles were obtained when DIW was used as a solvent, while the increase in power caused an increase in the nanoparticles' size. The FTIR measurements have shown the vibration patterns in the spectrum of the samples, indicating the formation of O-Ti-O.

The performance of the prepared samples for water treatment was studied using a standard photocatalytic degradation experiment. The Methylene Blue (MB) with a concentration of (10 ppm) in deionized water was used as a polluted system. All the

experiments were conducted under ultraviolet (UV) for (100 min) of exposure time. The highest removal of methylene blue from solution was observed with the DIW 60% sample, which reached about 64.22 % under UV irradiation during the exposure time. This is due to the increase in the surface area of the prepared sample.

List of contents

Subject	Page No.
Abstract	I
List of Contents	III
List of symbols	V
List of Abbreviations	VI
List of Figures	VII
List of Tables	VIII
Chapter One: Introduction	
1.1 General Introduction	1
1.2 Problem Statement	2
1.3 Aim and Objectives	3
1.4 Thesis Layout	3
Chapter Two: Fundamental Principles and Literature Review	
2.1 Introduction	5
2.2 Nanotechnology and Nanomaterials	5
2.3 Synthesis of nanostructured materials	8
2.3.1 Bottom-up approach	9
2.3.2 Top-down approach	10
2.4 Titanium dioxide (TiO_2)	10
2.5 Synthesis methods of TiO_2 nanoparticles	13
2.5.1 Microwave method	13
2.5.2 Sol-gel method	14
2.5.3 Hydrothermal method	15
2.5.4 Solvothermal method	15

Subject	Page No.
2.6 Related works	16
2.7 Principles of the Photocatalysis	22
2.8 Photocatalytic Mechanism of TiO_2	24
Chapter Three: Methodology	
3.1 Introduction	27
3.2 Materials	27
3.3 Synthesis of TiO_2 nanoparticles	27
3.4 Characterization techniques	30
3.4.1 X-Ray Diffraction (XRD) analysis	30
3.4.2 Specific Surface Area (BET)	32
3.4.3 Field Emission Scanning Electron Microscopy (FESEM) and Energy Dispersive X-ray Spectroscopy (EDX)	34
3.4.4 Fourier transform infrared (FTIR)	36
3.4.5 Ultraviolet-visible spectroscopy (UV-Vis)	37
3.5 Photocatalytic activity	39
Chapter Four: Results and Discussion	
4.1 Introduction	43
4.2 X-ray Diffraction Analysis	43
4.3 Specific Surface Area (BET) Results	46
4.4 FESEM Results	51
4.5 FT-IR results	61
4.6 Photocatalytic activity results	63
4.7 Conclusions	72
4.8 Suggestions for the Future Research	74
References	75

List of symbols

Symbol	Definition
A	Absorbance
Å	Angstrom (10^{-10} m)
A_o	Initial absorbance
C_o	Initial concentration (mg/L or ppm)
C_t	Concentration after a period of time (mg/L or ppm
^oC	Degree Celsius
d	Inter planer space
D	Average crystal size
D%	Degradation rate
e-	Electron
g	Gram
HO_2•	Hydroperoxyl radical
h+	Hole
ħ	Planck's constant
hr	Hour
hkl	Crystal plane indices
ħν	Incident photon energy
K	Kelvin
N_2	Nitrogen
OH-	Hydroxide ion
OH•	Hydroxyl radical
O_2	Oxygen
O_2 •	Superoxide radical
P	Pressure
P/P_0	Relative pressure
T	Temperature (ºC or K)
t	Time (sec or min)
W	Watt
θ	Bragg angle (degree)
λ	Wavelength of light
ν	Frequency of photon
β	Full-width at half maximum in radian

* Other symbols (not mentioned here) were defined during the text.

List of Abbreviations

BET	Brunauer-Emmett-Teller
BJH	Brunauer-Joyner-Halanda
CB	Conduction Band
CVD	Chemical Vapor Deposition
C_2H_5OH	Ethanol
DIW	Deionized water
DSSC	Dye-Sensitized Solar Cell
EDX	Energy Dispersive of X-ray spectroscopy
EG	Ethylene Glycol
eV	Electron Volt
FESEM	Field Emission Scanning Electron Microscopy
FT-IR	Fourier Transform Infrared Spectroscopy
FWHM	Full-Width at Half Maximum
IR	Infrared
MB	Methylene Blue
mL	Milliliter
μm	Micrometer (10^{-6} m)
nm	Nanometer (10^{-9} m)
pH	Acidity of an aqueous solution
rpm	Rotation rounds per minute
SEM	Scanning Electron Microscopy
TTIP	Titanium (IV) isopropoxide or Tetra-isopropoxide
UV	Ultraviolet
V_B	Valence Band
Vis	Visible light
XRD	X-ray Diffraction
0D	Zero-dimensional
1D	One-dimensional
2D	Two-dimensional
3D	Three-dimensional

* Other abbreviations (not mentioned here) were defined during the text.

List of Figures

Figure No.	Subject	Page No.
(2.1)	The exponential growth of nanotechnology.	6
(2.2)	Forms of nanomaterials by the size of their structural components.	8
(2.3)	Schematic of Bottom-up and Top-down approaches.	9
(2.4)	Crystal structures of TiO_2 : (a) anatase (b) rutile (c) brookite.	12
(2.5)	General mechanism of photocatalysis of TiO_2.	25
(3.1)	The microwave oven.	28
(3.2)	Steps of the synthesized samples.	29
(3.3)	The furnace (ELF 11/14B).	29
(3.4)	The schematic diagram for preparation process of TiO_2 nanoparticles.	30
(3.5)	A schematic representation of the Bragg law.	31
(3.6)	The X-Ray Diffraction.	32
(3.7)	The micromeritics of analyzing specific surface area.	33
(3.8)	Field Emission Scanning Electron Microscopy.	34
(3.9)	Schematic representation of the basic operation of a FESEM.	35
(3.10)	Fourier transform infrared spectroscopy device.	37
(3.11)	Beer-Lambert law	38
(3.12)	UV-Vis spectrophotometer device.	38
(3.13)	A photograph of the (a) photocatalytic setup and (b) reactor parts.	40
(4.1)	The X-ray diffractograms of the TiO_2 nanoparticles.	44
(4.2)	(N2) adsorption - desorption of anatase TiO_2 nanoparticles for (EG60%, EG80%, and EG100%) samples.	47
(4.3)	(N2) adsorption - desorption of anatase TiO_2 nanoparticles for (DIW60% and DIW80%) samples	47
(4.4)	The typical N2 adsorption-desorption isotherm of anatase TiO_2 nanoparticles for (EG60%) sample.	48
(4.5)	Pore size distribution of anatase TiO_2 nanoparticles for (EG60%, EG80%, and EG100%) samples.	49
(4.6)	Pore size distribution of anatase TiO_2 nanoparticles for (DIW60% and DIW80%) samples.	50
(4.7)	FESEM images of TiO_2 nanoparticles for EG60% sample.	52
(4.8)	FESEM images of TiO_2 nanoparticles for EG80% sample.	53
(4.9)	FESEM images of TiO_2 nanoparticles for EG100% sample.	54
(4.10)	FESEM images of TiO_2 nanoparticles for DIW60% sample.	56
(4.11)	FESEM images of TiO_2 nanoparticles for DIW80% sample.	57
(4.12)	EDX spectrum of TiO_2 nanoparticles prepared at EG60% sample.	58
(4.13)	EDX spectrum of TiO_2 nanoparticles prepared at EG80% sample.	59
(4.14)	EDX spectrum of TiO_2 nanoparticles prepared at EG100% sample.	59
(4.15)	EDX spectrum of TiO_2 nanoparticles prepared at DIW60% sample.	60
(4.16)	EDX spectrum of TiO_2 nanoparticles prepared at DIW80% sample.	60
(4.17)	FTIR spectrum of the prepared TiO_2 nanoparticles.	62
(4.18)	Absorbance spectra of MB versus wavelength without UV irradiation in the	64

	presence of the TiO_2 nanoparticles for DIW 60% sample.	
(4.19)	UV-Vis absorption spectra of MB solution after photocatalysis for EG60% sample with different reaction time.	65
(4.20)	UV-Vis absorption spectra of MB solution after photocatalysis for EG80% sample with different reaction time.	66
(4.21)	UV-Vis absorption spectra of MB solution after photocatalysis for EG100% sample with different reaction time.	66
(4.22)	UV-Vis absorption spectra of MB solution after photocatalysis for DIW60% sample with different reaction time.	67
(4.23)	UV-Vis absorption spectra of MB solution after photocatalysis for DIW80% sample with different reaction time.	67
(4.24)	Photocatalytic decolorization behavior of MB using prepared TiO_2 nanoparticles samples.	68
(4.25)	The first-order-kinetics of photocatalytic degradation of MB solution using the prepared TiO_2 nanoparticles samples.	71

List of Tables

Table No.	Subject	Page No.
(2.1)	Physical properties of TiO_2	12
(4.1)	XRD results for TiO_2 nanopowders at selected temperatures	45
(4.2)	The average crystallite sizes of the TiO_2 at selected temperatures	46
(4.3)	The Surface area, average pore size of TiO_2 nanoparticles samples prepared	50
(4.4)	The average lengths, diameters, and aspect ratio of TiO_2 nanorods	55
(4.5)	The quantitative details about the EDX analysis.	61
(4.6)	Summarize FTIR spectrum of the prepared TiO_2 nanoparticles.	63
(4.7)	The percent of obtained degradation after the photocatalytic reaction with the prepared TiO_2 nanoparticles samples.	69
(4.8)	First-order kinetic constants (k) for photocatalytic degradation using the prepared TiO_2 nanoparticles after 100 min of UV irradiation.	71

Chapter One

Introduction

1.1 General Introduction

Over the past decades, the industrial advancements have led to an increase in the water consumption rate. Due to the lack of clean water resources, water recycling via the elimination of exceedingly colored wastewater has become very important. The organic components such as phenols cause nasty taste and smell in water also it can extend negative effects on natural biological operations. While, the organic contaminants such as methylene blue (MB), benzene, carbon tetrachloride vinyl chloride, and trichloroethylene can cause health hazards if they exist in large quantities. These contaminants must be removed from polluted water if it has to be employed for in-home human consumption [1]. Different methods in this field such as oxidation, adsorption, anaerobic and reduction treatments have been developed for the elimination of contaminated dyes from the effluents. Unfortunately, these processes have many disadvantages such as expensive operating conditions, creation of sludge, time-consuming, and inefficiency in situations where complex aromatic compounds are produced [2].

Therefore, scientists and researchers are trying to discover and develop new methods for water treatment of organic compounds, such as dyes, via photocatalytic procedure using semiconductor degradation process. This process is cheaper, simpler, and cleaner. Hence, the process of photocatalysis is confessed as being a “greener” technology for toxic inorganic and organic pollutants elimination from wastewater at normal pressure and ambient temperature. Photocatalysis based on titanium dioxide (TiO_2) nanoparticles as a perpetual photocatalyst have received much attention among water purification technologies during the past years, due to its wideband energy, low cost, stable material, high activity, and nontoxic [3].

The photocatalytic efficiency of the TiO_2 depends on several factors such as the bandgap, the particles size, the crystalline structure, and the surface area. As well as, the efficiency of the materials can be further enhanced by doping [4]. The nanostructure materials have the best performance as a catalyst, electrical and optical properties [5].

The materials with the best photocatalyst must have a high surface area as well as high efficiency for photon conversion. Many researchers have focused their interest on increasing TiO_2 surface area to enhance the activity of the photocatalyst. The minimizing of the TiO_2 particle size to the nanoscale has been reported to ameliorate the photocatalytic process efficiency. The improvement occurs due to the TiO_2 nanoparticles having a greatly high surface area.

Many researchers have reported the preparation of TiO_2 nanoparticles using several ways such as sol-gel, hydrothermal, microwave-assisted methods, etc. However, most of these synthesis processes require multiple steps, long synthesis times, and demand expensive thermal equipment. Thus, there is a request to find a faster and easier method for preparation.

In recent years, the microwave synthesis has been widely used as it is a fast, energy-efficient, low temperature, and environmentally friendly process. Microwave irradiation performs a set of powerful, highly reliable, and selective reactions for the rapid synthesis of various shapes of TiO_2 nanoparticles.

1.2 Problem Statement

One of the most important fields of research in the present time towards the environmental applications is to prepare effective nanoparticles as catalysts via green and low-cost technology. The removal of organic dye from the wastewater by the photocatalytic procedures can be realized using titanium dioxide (TiO_2) nanoparticles. The attribute for using TiO_2 as supreme photocatalyst was its activity under UV irradiation. Due to it has a unique bandgap and the decreasing the size of the particle increases this bandgap. The photocatalytic activity of TiO_2 has been enhanced via

produced catalyst with high surface area and certain morphology. The increase in the surface area can be realized by controlling the catalyst morphology and forming the catalyst with a particle size in the nanometer scale. Thus, it is necessary to find the best preparation conditions if the smallest likely nanoparticles are to be obtained for these catalysts.

In this work, a faster and simpler process was used to prepare the nanocatalyst materials. This study also sought environmental applications of produced nanocatalyst via enhancement of MB degradation under ultraviolet (UV) irradiation by photocatalytic techniques.

1.3 Aim and Objectives

A simple process, the microwave method, was used in this study for preparing the samples. The main objectives of this thesis are:

1- Synthesis of TiO_2 nanoparticles by Microwave method.

2- Characterizations of the TiO_2 nanoparticles by XRD, FESEM-EDX, BET, and FT-IR analysis.

3- Study of the effect of different solvents with different microwave powers on TiO_2 nanoparticles properties.

4- Study of the photocatalytic activity of TiO_2 nanoparticles towards water purification processes.

1.4 Thesis Layout

This thesis consists of four chapters. Chapter 1 is a general introduction, the problem statement, and the aim. Chapter 2 describes the fundamental principles and literature review which shows an overview of the nanotechnology and nanostructured materials, the synthesis of nanostructured materials, the brief background of TiO_2 and its crystal structure as well as the preparation methods of TiO_2 nanoparticles. The chapter also explains an introduction to the basic principles of the photocatalysis. The end of this

chapter illustrates the photocatalytic mechanism of the TiO_2 semiconductor. Chapter 3 is the methodology that describes in detail the selected precursor materials and the process to produce TiO_2 nanoparticles. The fundamental principles of techniques, which were utilized to characterize the synthesized samples, are briefly clarified. Finally, the experimental setup for the TiO_2 photocatalytic activity test will be elaborated at the termination of this chapter. Chapter 4 describes the finding on characterizations of TiO_2 nanoparticles. In addition, the photocatalytic activity of synthesized TiO_2 nanoparticles was estimated using the organic methylene blue (MB) degradation experienced under UV irradiation. Finally, the chapter gives the conclusions and the recommendations for future work.

Chapter Two

Fundamental Principles and Literature Review

2.1 Introduction

In this chapter, an overview of nanomaterials is presented. The detection, classifications, and the approaches to nanostructure materials formation are discussed. The preparation methods of Titanium dioxide (TiO_2) nanoparticles and the literature review of the related work have been explained. Several methods have been employed to prepare TiO_2 nanopowders, such as sol-gel [6], solvothermal, hydrothermal [7], and microwave processes [8].

In previous years, among the metal oxides nanostructures, Titanium dioxide (TiO_2) has been widely studied and used in many applications due to its unique and promising properties [9]. Its function as a friendly photocatalyst has also observed wide applications to problems of the environment such as wastewater treatment and purification of contaminated aqueous solutions. Titanium dioxide (TiO_2) has become the best material for photocatalytic activities due to its photo-corrosion resistance, abundance, low cost, and non-toxicity [10].

2.2 Nanotechnology and Nanomaterials

The "Nano" is a term that originated from the Greek nano which means dwarf. It is one-billionth of a meter. It's related to nanoscience and nanotechnology. This branch of science and technology deals with materials having at least one dimension in the size range of 1 to 100 nm. The term “nanotechnology” was firstly used in 1974 by Norio Taniguchi. This name belonged to an ion sputtering machine which means getting extra-high precision and ultrafine structure in nanometer [11].

Nanotechnology can be defined as the design, configuration, characterization, and production of materials as well as instruments and systems by controlling the size and shape of a nanometer scale. Nanotechnology can introduce new substances of various chemical, physical and biological properties, including nanomaterials [12]. As a consequence, in different fields such as microchip technology, medical and scientific research, nanotechnology has been used. The last years had visible exponential growth in the field of nanotechnology and nanomaterials as shown in figure (2.1). Scientists and researchers are working to improve techniques where structures and devices with nanoscale composition could be fabricated at a wide-range and with reasonable cost [10].

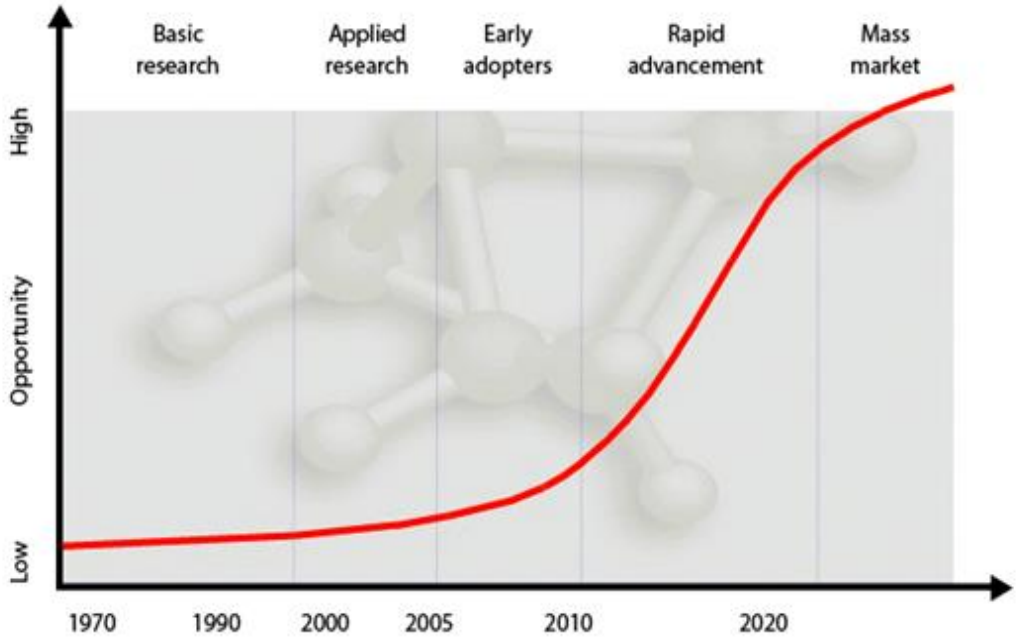

Figure (2.1) The exponential growth of nanotechnology [11].

These nanostructured materials have gained the interest of recent science and technology due to the increased ability to manufacture them. The nanomaterials are growing in interest compared to their counterparts in the bulk state because of their promised applications and unique properties. Nanomaterials are used in many applications, such as medical, automotive, electronic devices, food, and some consumed products [13].

Despite the recent development in the synthesis and characterization of variant nanostructures materials, many challenges remain due to properties of nanomaterials dependence on the control of size and shape, which created unmatched behavior if it's compared with the bulk materials [14]. Moreover, the characteristics of nanomaterials can also be wildly different from the characteristics of materials in bulk types. When it comes to nanoparticles or nano-scale materials "size matters", they have a larger surface area than a bulk per unit-volume because the chemical processes of solids happen on such surfaces and thus more surfaces have been received. This means greater chemical reactivity whereas big-scale materials are measured by the characteristics of their bulk size that have a smaller surface area in comparison with the same materials in nano-scale. The particle size and shapes of crystals such as rods, spheres, tubes, fibers can have a larger shift in physical properties like optical and electrical properties [12].

The nanostructures can be categorized into three groups depending on the degree of freedom. Zero-dimensional (nanostructures indicate that all three dimensions are in nanoscale such as nanoparticles, quantum dots, nanospheres). One-dimensional (the structures have two nanoscale dimensions such as nanorods, nanotubes, and nanofibers). Two-dimensional (the crystalline structure that confined to one-dimension nanometer scales like nanosheets, nanoplatelets, and nanofilms). Three-dimensional structures (are distinguished that the dimensions exceed the nanometer scale (large than 100 nm such as bulk materials). These shapes of the particle change the physical attributes of the materials as shown in figure (2.2) [15, 16].

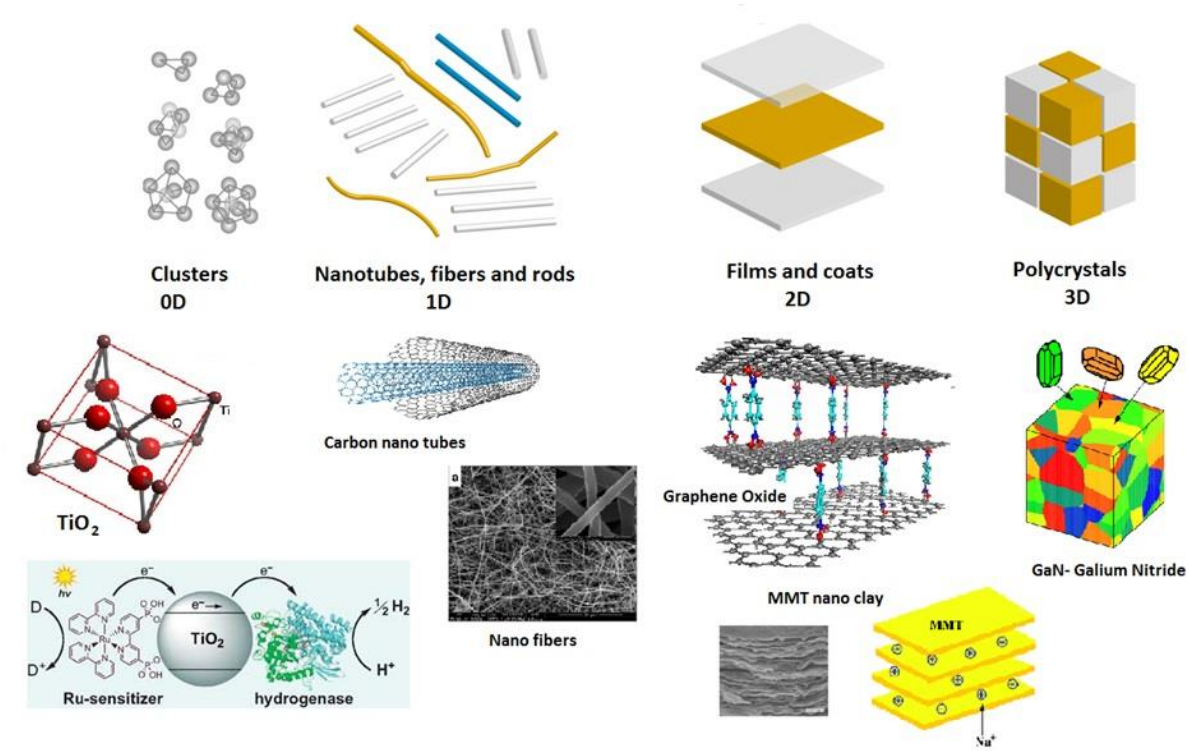

Figure (2.2) Forms of nanomaterials by the size of their structural components [16].

2.3 Synthesis of nanostructured materials

Nanotechnology is the investment of material at molecular and atomic levels. Synthesized materials can be arranged in useful forms in order to finally apply the material to a particular application. Synthesis techniques for producing metal nanoparticles rely on the isolation of small quantities of a substance. Figure (2.3) shows the two basic approaches for having nanoscale materials "bottom-up" and "top-down".

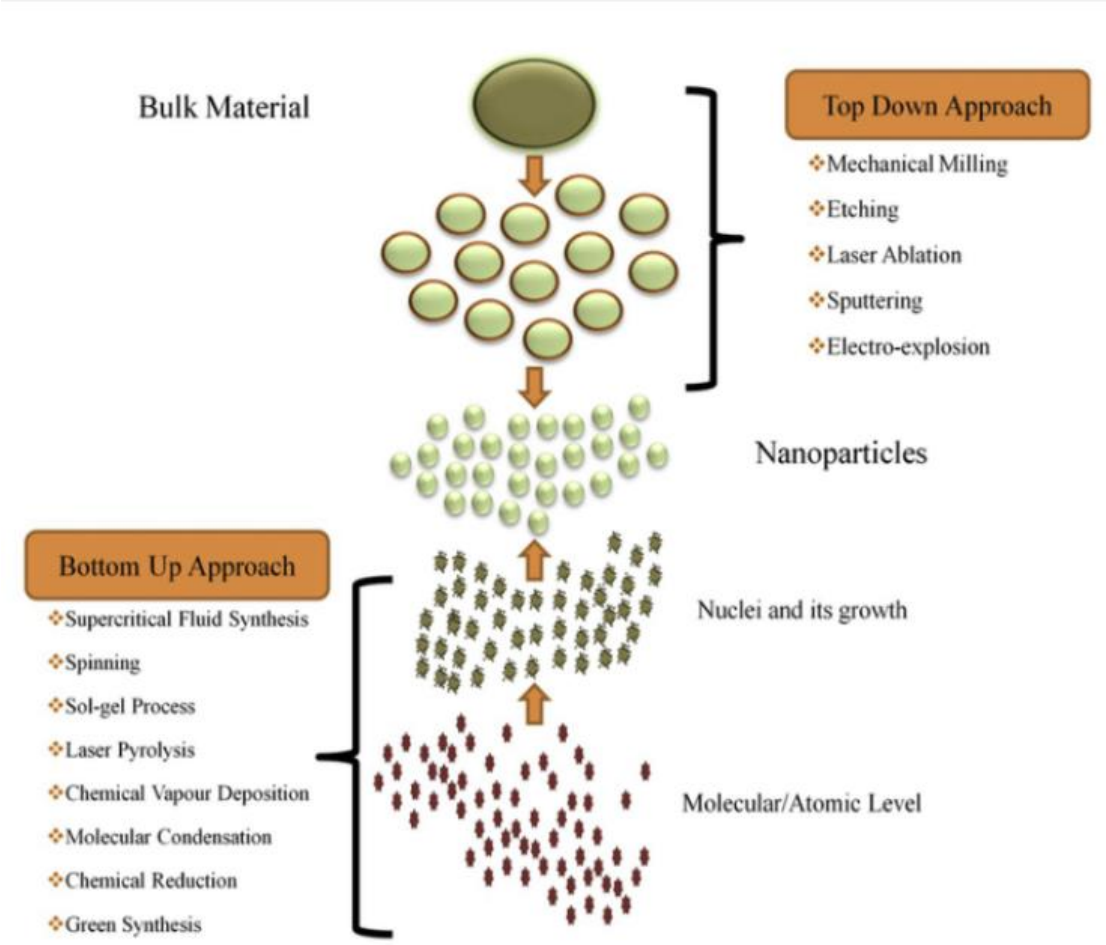

Figure (2.3) Schematic of Bottom-up and Top-down approaches [17].

3.2.1 Bottom-up Approach

The bottom-up approach implicates self-assembly to nano production by the employment of physical and chemical forces operating at the nanoscale to compile smaller singularities to create larger structures; examples of the bottom-up approaches are self-assembly, chemical synthesis, and molecular fabrication. This technology usually is able to fabricate instruments in counterpart to the much cheaper than technologies of top-down. In other words, it is similar to building a house, by taking many building blocks and gathering them together to make the final greater structure [17].

3.2.2 Top-down Approach

The process that onsets from a big part (bulk materials) and then utilizes precise tools to produce correspondingly smaller structures (nanostructure) is known as the top-down approach. The top-down approach can usually realize good control over the instrument dimension, location, and organization with high precision. There are several techniques to achieve this approach such as:

Mechanicanosynthetic methods present a cheaper way to fabricate nano-materials in bulk. The simplest of them is ball milling. Ball milling fabricates nanomaterials by mechanical attrition that transfers the kinetic energy from a grinding medium to a material that is subjected to reduction. Compaction and consolidation are manufacturing-grade processes in which nanomaterials are "put back together" to configure materials with reinforced properties. Metallic alloys can be fabricated in this way. Various top-down mechanical methods are widely used by the industry.

In addition, there are several techniques to achieve this approach such as etching, milling, cutting, electrospinning, high energy methods, thermal methods, Laser ablation, chemical fabrication methods, and lithography. The lithography techniques such as photolithography, electron beam lithography, the concentrated ion beam lithography, and dip-pen lithography are getting much important to obtain the nanostructure. This technique has been beneficial to many fields such as software, powerful computers, and advanced devices [18].

2.4 Titanium Dioxide (TiO_2)

Titanium dioxide (TiO_2) also known as Titania, is a white inorganic solid substance that is indissoluble in water, thermally stable, chemically inactive, and non-ignitable. TiO_2 is vastly used in manufacturing applications like catalyst support, dye-sensitized photoelectrochemical solar cell, in consumer vendibles (cosmetics, coatings,

paints, ceramics, printing inks, textiles, etc.). In addition to the strong oxidizing power of the photogenerated holes and the non-toxicity of TiO_2 has also made it a superior photocatalyst [19]. Titanium dioxide belongs to the family of transition metal oxide. TiO_2 usually does not exist in nature but is derived from leucoxene ores or ilmenite. Titanium (the ninth most common element in the earth's crust) is found as a compound in several kinds of rocks and mineral sands [19, 20].

Compared to bulk material, the properties of TiO_2 nanostructured material show a strong dependence on size. The nanostructured TiO_2 possesses a large surface area for adsorption and catalysis. There are three common phase structures of TiO_2: brookite, anatase, and rutile. There are several different species of TiO_2 that can be obtained such as columbite, hollandite, ramsdellite. These composites don't exist in nature but they can be prepared in the laboratory at specific pressure treatment on anatase and rutile phase. Among these crystal structures, the anatase form shows the best photoactivity. The electron-hole recombination rate of rutile is higher than anatase; this may be one of the explanations that anatase performs photocatalytic reactions better than rutile. The difference of bandgap energy between anatase and rutile cannot be considered as one of the explanations, since the difference is too small. Moreover, anatase also performs photocatalytic reactions better than brookite. Since rutile is the most thermodynamically stable phase, the synthesis of phase pure anatase photocatalyst is challenging. Table (2.1) shows the general properties of these forms. TiO_2 is photostable, inexpensive, chemically, and biologically inert, high activity at ambient temperature and safe for use, and ideal to degrade trace-level pollutants [21].

Table 2.1 Physical properties of TiO_2 [21]

Crystal Structure	Anatase	Brookite	Rutile
Crystal System	Tetragonal	Rhombohedral	Tetragonal
Density (g/cm3)	3.9	4.13	4.17
Band Gap Energy (eV)	3.2	3.1-3.4	3.0
Melting Point (℃)	Transform to Rutile	Transform to Rutile	1870
Refractive Index	2.52	2.63	2.72

Figure (2.4) displays the various phases of TiO_2, with various phase structures that may be different in the chemical and physical properties of the total material.

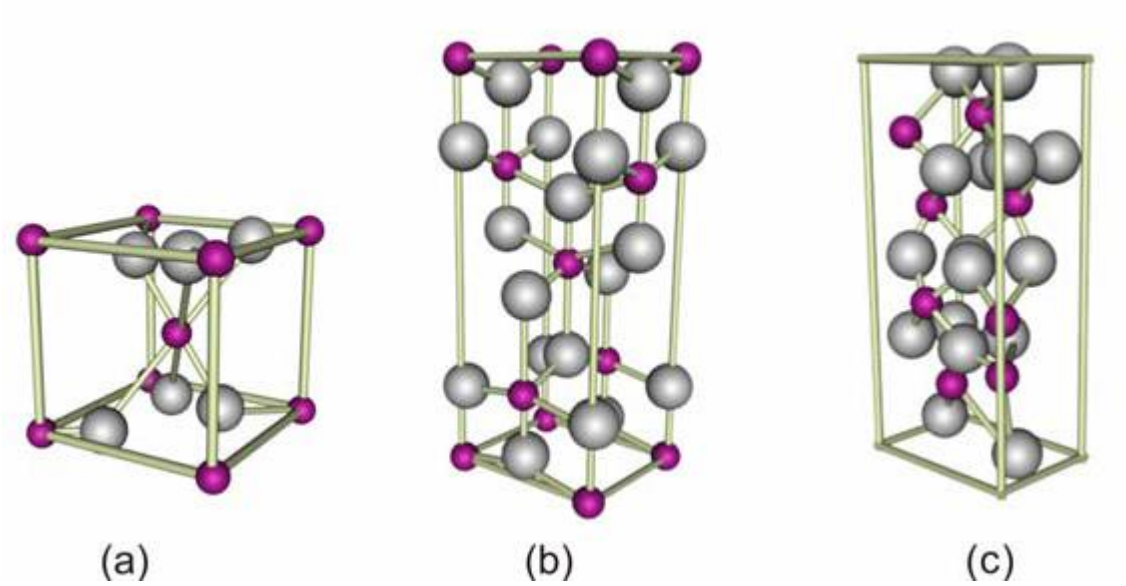

Figure (2.4) Crystal structures of TiO_2 : (a) Anatase (b) Rutile (c) Brookite [22].

The titanium oxide rutile phase is a tetragonal crystalline structure (with prismatic habit). It is primarily applied as a white tincture in varnish. The Titanium oxide anatase formulation is a tetragonal crystalline structure and it is applied as a photocatalyst

under ultraviolet irradiation due to its bandgap energy of 3.2 eV. The Titanium oxide brookite phase is an orthorhombic crystalline structure [20].

2.5 Synthesis Methods of TiO_2 Nanoparticles

In order to synthesis Titania and apply it in the photocatalytic activity, the physiochemical properties must be controlled (size, morphology, and composition). By utilizing specific methods to get photocatalytic activity with the required properties. TiO_2 nanoparticle properties in nano-powders form significantly depend on some parameters such as the morphology, crystalline phase, specific surface area, and porosity, which in turn depend on the method of preparation. The most important factors for the enhancement of the catalyst activity are the porosity and the specific surface area of the materials, which are achieved by controlling the TiO_2 nanoparticles' shape, morphology, and size. Furthermore, the synthesis of Titania has to be environmentally friendly, fast, and low cost [20]. TiO_2 nanorods, nanowires, nanofibers, nanotubes, nanosheets, nanoplatelets, and spherical nanostructures have been prepared by using numerous methods. Recently, TiO_2 nanorods have attracted extensive attention for their probable application in photocatalytic activity with a high response to ultraviolet (UV) light. These are due to the nanorod structure has exhibited faster generating (electron-hole) pairs and a lower rate of recombination [23]. Several preparation methods have been studied for the synthesis of Titania such as microwave, sol-gel, hydrothermal, and solvothermal, etc.

2.5.1 Microwave Method

Microwaves are electromagnetic waves that are positioned between infrared (IR) and radio waves with a frequency range of (0.3 – 300) GHz. The essential microwave frequencies are between (900 - 2450) MHz with a wavelength of nearly (12.24) cm. Microwave heating is done by electromagnetic waves where they are absorbed directly via the molecules of material by having a dipole moment that leads to growing their

temperature. The dipole of the molecules rotates aligning itself with the external electric field due to its sensitivity [20].

The heating mechanism of the microwave differs from conventional heating. In microwave heating, the interaction between the electromagnetic waves and the material generates homogeneous internal heating. While in conventional heating, the heating begins with the surface of the utensil, and then by the thermal conduction, it reaches all the material. This heating mechanism takes a longer synthesis time and higher energy than microwave heating (the temperature of the utensil is higher than the material), and the materials are not uniformly heated [24].

In recent years, microwave synthesis has been widely used by many researchers as it is a fast, energy-efficient, low temperature, and environmentally friendly process. Microwave irradiation performs a set of powerful, highly reliable, and selective reactions for the rapid synthesis of various shapes of TiO_2 nanoparticles [21].

2.5.2 Sol-gel Method

The sol-gel process is a multilateral simple chemical process. To a large degree, it is used for the preparation of ceramic metal oxides and glass materials. The sol-gel process can usually include the employment of inorganic salts or metal alkoxides as progenitors. In this method, the progenitors subject a spectrum of hydrolysis and polycondensation motivation to compose a colloidal amputation or a sol. This method includes the transmission procedure into a solid “gel” state from a liquid “sol” (mostly "colloidal") state, then the gel is dried to gain the metal oxide nanopowder by calcification at various temperatures.

The sol-gel process has major advantages such as the potential of gaining unstable materials, the difference to high-temperature processes, obtaining excellent purity and the structure of the product is homogenous at modest temperatures. Moreover,

this method also affects the morphology of the particles pending the chemical transmutation of the molecular predecessors to the ultimate oxidic grid [18].

2.5.3 Hydrothermal Method

The hydrothermal interaction is conducted in a steel pressure vessel, as a rule, a utensil which is known as "autoclave" with Teflon underlay, under controlled pressure or controlled temperature with the interaction in aqueous solutions [7].

The autoclave is placed inside an oven at a temperature that can reach 250 ºC. Due to the use of autoclave in this method, the temperature of the interaction can increase upon the boiling point of water, amounting to the saturated water vapor pressure. Two temperature regions were created inside the utensil. The material will dissolve in the lower part (hotter part) of the autoclave. While the saturated aqueous sol is transferred to the upper part (colder part) of the autoclave. Therefore, the crystallization process starts. This method usually uses less temperature than the solid-state reaction.

The amount of solution and the temperature that was added to the "autoclave" usually predestine the internal pressure created. The hydrothermal process is known as any nonhomogeneous interaction to resolve and re-crystallize the material which is middling unsolvable under average conditions [20].

2.5.4 Solvothermal Method

This method slightly differs from the hydrothermal process with the existence of a particular solvent. In this process, a specified solvent is utilized that is non-aqueous in nature. This method uses several organic solvents that have a higher temperature and elevated boiling degrees compared to the hydrothermal process. In the solvothermal process, more advanced domination on the compose distributions, size, and crystallinity of the TiO_2 nanopowder is obtained. This process is applied for the production of nanoscale metals, ceramics, polymers, and semiconductors by utilizing solvent under

elevated to mild pressure. It's a variable process for the production of an assortment of nanoparticles with paltry size distribution and dispersity. Therefore, the solvothermal method is known as the hydrothermal method when water is used as the solvent in the synthesis.

2.6 Literature Survey

Carlucci, et al. [25] (2014) have synthesized anatase TiO_2 nanorods by Titanium isopropoxide TTIP with acetic acid and benzyl alcohol at 210 °C via the microwave-solvothermal method for 45 min. The HR-TEM results showed that the nano-crystals shape varies from small spherical (size about 5 nm) to nearly spherical (slightly elongated) to rod-like (5 nm diameter and 10 nm in length). The BET results showed a high surface area which makes better photocatalytic performance. It was concluded that the TTIP: acetic acid ratio controls the crystalline quality and morphology.

Moura, et al. [26] (2014) prepared anatase titanium dioxide TiO_2 by using a microwave-assisted solvothermal method and it was done using TTIP and ethanol. The synthesis was done under pressure of 200 kPa and heated by microwave radiation at 120 °C for five different reaction times (1, 5, 15, 30, and 60 min). SEM results showed micro-spherical morphology after 1 min reaction time while a change in morphology (spheres and sticks) was observed after a 60 min reaction time. It appeared that by increasing the reaction time, the crystallite size has also increased.

Xu, et al. [27] (2014) synthesized ultrafine anatase titanium dioxide TiO_2 via a microwave solvothermal method by using three different molar ratios of TTIP : glucose with benzyl alcohol. The solution was placed in a microwave oven (600 GHz) at 210 °C, 60 atm for 45 min. The results showed irregular shape morphology. It was concluded that the concentration of glucose controlled the size and the morphology of the nanoparticles.

Lu, et al. [28] (2014) synthesized anatase TiO_2 nanoparticles at high pressure by hydrothermal method (direct heating), microwave-assisted hydrothermal method (indirect heating), and regular sol-gel method. TTIP was mixed with deionized water, hydrochloric acid, and ammonia hydroxide for pH adjustment. The characterization results showed the average size of TiO_2 was 5.72 nm for the microwave-assisted method, 7 nm for the hydrothermal method, and 13.71 nm for the sol-gel method. It was concluded that one of the main factors to control the size of TiO_2 nanoparticles was the pH value while the microwave-assisted method had better control on the size of the nanoparticles below 10 nm which justified the effectiveness of photoreactivity under neutral conditions.

E. Filippo, et al. [29] (2015) synthesized pure anatase titanium dioxide TiO_2 from TTIP, acetic acid, benzyl alcohol, and chloroplatinic acid by using a microwave method at a frequency of 2.45 GHz and a temperature of 200 °C for 45 min. The TEM images showed slightly elongated (rodlike) nanoparticles with an average length and width of 13.8 ± 5.5 nm and 9.0 ±1.2 nm respectively. BET results showed a specific surface area around 89.46 m^2g^{-1} and an average pore size of 2.9 nm. The photocatalytic evaluation demonstrated excellent performance.

Mohadesi and Rnjbar [30] (2016) prepared pure TiO_2 nanoparticles by dissolving TTIP in distilled water and Nitric acid by using a microwave method, with two powers (600 and 750 W) and different times (4, 6, 8, 10 min). Through XRD, SEM, and TEM, it has been observed that the increase in power and time has also increased the crystallinity, particle size, and agglomeration, and the morphology changed from nanoparticle to micro-sphere with a size of about 30-40 nm. The PL results showed that the emission spectrum includes a single distinct peak at 405 nm.

Ranjan, et al. [31] (2016) prepared TiO_2 nanoparticles by a microwave-assisted hybrid chemical approach. It was synthesized with a laboratory microwave oven at (400W) from TTIP, acetonitrile, and urea. The annealing process was done in two steps,

first, in a microwave oven at 1000 W for 1 h, then in the air using a muffle furnace at 300 °C for 1 h. SEM images showed the monodispersity of the nano titania and the absence of agglomeration with an average size of (28.3 ± 3.1 nm). It can be noted that the microwave-assisted hybrid chemical approach is decreasing the synthesis time.

Joshi, et al. [32] (2016) synthesized direct anatase phase mesoporous TiO_2 by using a microwave-assisted sol-gel method at low temperatures. The process involved a reaction between TTIP, nitric acid, and Millipore water, for 10 min at 80 °C. It was annealed at 450 °C for 30 min then at 500 °C for 30 min. The average crystalline size was around 6 nm. SEM results showed TiO_2 nano-aggregates with an average particle size of ~300-400 nm. BET results showed the surface area around 135 m^2/g before annealing and 95 m^2/gm after annealing, with an average pore size of 2-4 nm.

Su, et al. [33] (2016) prepared pure anatase titanium dioxide TiO_2 with high thermal stability by using a microwave-assisted hydrothermal method at 200 °C for 20 min. The nanoparticles were annealed under air atmosphere at different temperatures (from 400 to 1000 °C) for 2 h. The change in the annealing temperature caused a change in the anatase-to-rutile phase transformation. SEM and TEM images showed the morphology varying from sphere to polygon with an average size of 20 - 85 nm.

Cabello, et al. [34] (2017) synthesized anatase titanium dioxide TiO_2 nanoparticles from titanium isopropoxide (TTIP), polyethylene glycol, and sulfuric acid. Via fast microwave-hydrothermal route under microwave conditions at 240 °C for 20 seconds under a pressure of 25 bar. SEM images showed spherical-shaped particles with an average diameter of 100 nm and appeared as aggregates. BET analysis suggested high roughness particles with a relatively high surface area of 83 $m^2 \cdot g^{-1}$, containing small pores (2.6 nm).

Santhosh, et al. [35] (2017) successfully prepared nanospheres soporous titanium dioxide TiO_2 by using a microwave-assisted hydrothermal method from TTIP, ethanol, and Millipore water. It was placed in a microwave oven that was heated at 140 ºC for 1 hour, after that it was sintered at 450 ºC for 2 hours. XRD results showed a mixture of anatase and brookite phases with an average crystalline size around 8 nm. BET results showed it has a surface area of 87 m^2g^{-1} with an average pore size of 11.2 nm.

Bregadiolli, et al. [36] (2017) synthesized TiO_2 nanoparticles by a microwave-assisted hydrothermal method in alkaline and acidic mediums using mild conditions with TTIP as a precursor with different concentration and was stirred for 6 h at 80 °C, the solution was positioned in a microwave oven at a range of temperatures from 110 °C to 150 °C with a preparation time from 2 to 60 min. When the acidic solution was synthesized, the morphology of the nanoparticles shows irregular spheres while the structure was nearly the same. However, when the alkaline solution was synthesized, the Na+ ion concentrations had a high effect on the morphology and the growth of the nanoparticles which showed needle-like structures in addition to aggregated nanotube-like structured (after 30 min of synthesis). The XRD results showed the anatase phase with the presence of the brookite phase. Besides that, a high surface area was obtained, in the acidic medium, the surface area was 207 m^2/g, while in the alkaline medium it was 375 m^2/g.

Firas K. Mohamad, et al. [8] 2018, prepared hollow-spherical mesoporous Titanium Dioxide (TiO_2) nanostructures in a pure anatase phase using a microwave-assisted method. TTIP was added into a vessel that contains ethanol under stirring for 3h at room temperature. Then, the mixture was put in a microwave oven at half (50%) the maximum power which is 1100W for 5 min. The synthesized product was collected and dried, then it was calcined for 1h in air at 500º C. It was observed that the product had an average size in a range between 200 – 500 nm, an average diameter of 8 nm, a pore size

of 2 – 50 nm, an approximate specific surface area of 172.3 m^2g^{-1}, and high photocatalytic efficiency for methylene blue degradation.

Anitha, et al. [37] (2018) synthesized nanoparticles of titanium dioxide TiO_2 via microwave-assisted solvothermal method using TTIP and acetic acid as a precursor with medium power at 70 ºC, pH value was adjusted to 10. XRD pattern indicates the anatase TiO_2 structure with an average crystallite size of 12 nm. SEM and TEM images displayed the uniform morphology in the form of nanoclusters with a range of particle sizes from 10 to 20 nm. From the UV-Vis spectra, the optical properties of TiO_2 were studied, the absorption peak was nearly 323 nm, and the bandgap of TiO_2 was 3.15 eV.

Guel, et al. [38] (2019) synthesized titanium dioxide TiO_2 with a solution of TTIP, propanol, and either hydrochloric acid or acetic acid by using microwave-assisted sol-gel at a power of 400W and temperature of 80°C with three preparation times (15, 30, and 60 min). Then the gel was calcined at 400◦C for 3 h. It was observed that the phase transformation was affected by using hydrochloric acid as catalyst and it was shown in the XRD results as rutile, anatase, and brookite with crystallite size in the range of (9 – 16 nm), while by using acetic acid as catalyst, only anatase phase was found with a crystallite size of an average between 11 and 22 nm. The results of SEM showed different sizes and irregular shapes particles for both samples. The measured surface area was 112.3 $m^2\ g^{-1}$ and 89.5 $m^2\ g^{-1}$.

Vinodhini, et al. [39] (2019) prepared titanium dioxide TiO_2 nanostructures from TTIP and polyol medium of glycerol. The solution was heated in a microwave oven of 2.45 GHz with four different powers (240 W, 480 W, 720 W, 960 W) and was annealed at 450 ºC for 3 hours. The different power densities affected the TiO_2 morphology, at 240 W it appeared as spheres, at 480 W it resulted in the one-dimensional growth (rodlike) with a diameter of 33 nm, at 720 W it appeared as a combination of rodlike and spherical nanoparticles which are nucleated on the surface of the rods, at 960 W it changed to a

three-dimensional flower-like structure. The pure anatase phase was observed only at 480 W while anatase with secondary rutile phases was observed at the other powers. The crystallite size was not affected by the increase in microwave power.

Almashhori, et al. [40] (2020) synthesized (anatase/rutile) TiO_2 nanoparticles by using a microwave-assisted sol-gel method with three different concentrations of TTIP and nitric acid as the structure-directing agent (the increase in Ti concentration caused an increase in the rutile phase ratio). The mixture was placed in a microwave oven at 100 °C and 700 W for 1 h, then it was dried and calcined at 500 °C for 4 h in air. From TEM images the results showed the morphology of the most particles were spheres with non-uniform sizes. The average particle size of the three samples was 35.04 ± 2.69, 35.17 ± 2.25, and 35.49 ± 1.89 nm with crystallite sizes in the range of 30 – 70 nm. It was concluded that the increase in the concentration of the anatase phase ratio caused a higher efficiency in the photodegradation and the antibacterial.

Ayyaz, et al [41] (2020) prepared titanium dioxide TiO_2 nanoparticles using the sol-gel method at room temperature from TTIP, isopropanol, and nitric acid. The obtained gel was heated for 2 hours at 300 °C to dry out the organic content. The synthesized nanoparticles were put in an incompletely vacuumed chamber for microwave plasma treatment for 5 min. It was shown in the XRD results of TiO_2 as anatase and rutile phases with particle size in the range of 0.2 to 14 nm. The SEM results showed trigonal and aggregated shapes. After plasma treatment, the size of the nanoparticles almost reduces by half. This method enhanced the photocatalytic activity of TiO_2 nanoparticles.

Nikabadi and Khosroabadi [42] (2020) prepared anatase and rutile Titanium dioxide (TiO_2) nanoparticles via a microwave-assisted solvothermal method using (TTIP), polyvinylpyrrolidone (PVP), and Ascorbic Acid (AA) in ethanol. The mole ratio of PVP/AA was found to be critical in determining the morphology and crystal phase of the final product. PVP/AA mole ratio varied from 1 up to 15 to obtain different

morphologies of TiO_2. The microwave irradiation treatment was for 5 min at 450 W. The microwave treated solution was transferred to a Teflon sealed autoclave for solvothermal synthesis and treated at 150 °C for 2 h. The obtained powder was washed and calcined at 400 °C. TEM images demonstrate nanoparticles with a narrow size of about 20 nm. SEM images showed they have uniform size distribution with uniformly long and narrow rod and nanowire structure with several micrometers' length and 35 – 45 nm thickness. TiO_2 nanoparticles and nanorods have been prepared with good photocatalytic properties.

P. Imoisili, et al [43] (2021) successfully prepared Vanadium and silver co-doped titanium oxide ternary nanocatalyst ($V/Ag/TiO_2$) via a microwave-assisted sol-gel method using $Ti(C_4H_9O)_4$, NH_4VO_3, and $AgNO_3$ as precursors. The solution was placed in the microwave oven for 2 min at a frequency of 2,450 MHz and 1,000 W. Then the product was dried and calcined at 350°C for 1h. The XRD analysis of the prepared TiO_2 and $V/Ag/TiO_2$ shows lattice fringes for both anatase and rutile crystalline phases. The BET results reveal a large surface area of 92.8 and 84.8 m^2g^{-1} for TiO_2 and $V/Ag/TiO_2$, respectively. The SEM images portrays a cluster of rod-like aggregate particles, while the HRTEM analysis illustrates nanoparticles of rod-like cylindrical shape with a homogeneous size diameter. The synthesized nanoparticles demonstrated a different photocatalytic degradation ability of Methylene Orange (MO) and Methylene Blue (MB) for both samples, which was significant for the $V/Ag/TiO_2$ sample, and poor for the TiO_2 sample.

2.8 Principles of the Photocatalysis

The photocatalysis expression consists of a combination of photochemistry and catalysis, this means that the light and the catalyst are necessary to enhance a chemical reaction [44]. The fundamental difference between the photocatalytic reaction and the traditional catalyst reaction is that the catalyst material is activated under light other than by heat. Photocatalysis can be defined as the material that accelerates the rate (time and

speed) of the chemical reaction. It does not change in itself or get consumed in the reaction under visible light and ultraviolet irradiation [45]. Photocatalysts are classified into two types, the homogeneous photocatalysts and the heterogeneous photocatalysts depending on the photo-catalyst phase with the reaction components.

The homogeneous photocatalysts are called when they are in the same phase with the materials involved in the chemical reaction which usually are dissolved in the reaction mixture. Metal salts, bases or acids, solvents, radical initiators, and enzymes are examples of this type. Whereas the heterogeneous photocatalysts are different in the phase with the reactants and typically do not dissolve in the solvents. Examples of this type including solid acids and bases, supported metals, sulfides, and immobilized enzymes. Therefore, the heterogeneous photocatalysts are impenetrable materials unless they have a porous structure [46].

In the homogeneous photocatalyst, a powerful ultraviolet (UV) lamp is used for illuminating the polluted water in the existence of O_3, Fe^{+3}, or H_2O_2. The presence of such elements runs out as a catalyst and the reaction occurs in the bulk solution. On the other hand, the heterogeneous photocatalyst takes place with one or more interaction steps which mean the generation of electron-hole pairs via an appropriate light on the surface of semiconductor solid materials. The distribution and employment of incident light energy due to the existence of solid catalyst material in a gaseous or liquid mixture, make this procedure much complex compared to homogeneous procedures [47].

The performance of semiconductor photocatalysts significantly depends on their physical properties such as the morphology, the specific surface area, the crystalline structure, the surface density of the hydroxyls groups, and the particle aggregate size [48]. In the past decades, the concern has been focused on the process of oxidation especially the utilization of semiconductor metal oxides to remove the organic and inorganic pollutants [49].

The heterogeneous photocatalytic process of oxidation using TiO_2 extradited more attention as an alternative process for both water and air purifications [50]. The main feature of the heterogeneous photocatalyst, that there are no remains of the original material. That means, no sludge residue requires disposal due of the process breaks down the pollutants into harmless products such as CO_2 and H_2O [51].

The initial process in heterogeneous photocatalyst materials is the formation of electron-hole pairs. When a semiconductor material is irradiated with a photon having energy (hν) equals or higher than bandgap value, an electron (e^-) is elevated from the valence band (VB) to the conduction band (CB) and leaving a positive hole (h^+) in the valence band.

2.9 Photocatalytic Mechanism of TiO_2

The photocatalytic mechanism of TiO_2 starts from photon absorption with energy equal to or more than the value of the TiO_2 bandgap. Then, the electrons in the valence band (VB) would jump into the conduction band (CB) leaving an equal quantity of positive charges (holes) in the valence band (VB) as shown in figure (2.5). Therefore, when the photons were absorbed, the electron-hole (e^--h^+) pairs are produced in TiO_2. The excited state (e^--h^+) pairs can be recombined and dissipate the falling energy as heat or obtain trap in the surface, or react with donor and accepter electrons that adsorbed on the surface of semiconductor [52]. Generally, the absorbed water or hydroxide ions (OH^-) on the surface of TiO_2 can react with a hole (h^+) in the VB to produce hydroxyl radicals ($OH^\bullet$) with high oxidizing potential.

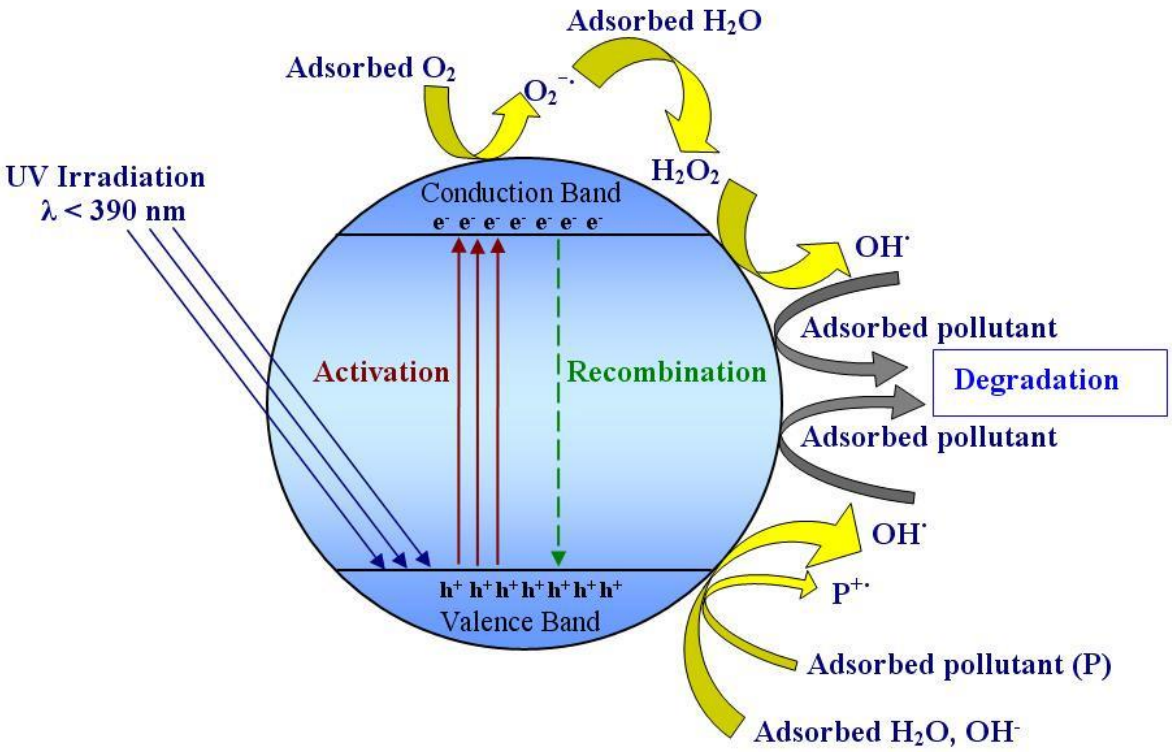

Figure (2.5) General mechanism of photocatalysis of TiO_2 [53].

While the electron (e^-) in the CB can reduce the oxygen (O_2) in its surroundings to generate superoxide radicals ($O_2^{\bullet-}$). The produced radicals will oxidize the methylene blue (MB) directly on the TiO_2 surface [54]. The steps of photocatalytic oxidation and reduction reactions of TiO_2 catalyst can be summarized in equations (1-6) [55].

$$TiO_2 + hv \rightarrow TiO_2 + {e_{cb}}^- + {h_{vb}}^+ \quad \ldots\ldots (1)$$

$${h_{vb}}^+ + OH^- \rightarrow OH^\bullet \quad \ldots\ldots (2)$$

$${h_{vb}}^+ + H_2O \rightarrow OH^\bullet + H^+ \quad \ldots\ldots (3)$$

$${e_{cb}}^- + O_2 \rightarrow {O_2}^{\bullet-} \quad \ldots\ldots (4)$$

$${e_{cb}}^- + H_2O_2 \rightarrow OH^\bullet + OH^- \quad \ldots\ldots (5)$$

$$H_2O_2 + {O_2}^{\bullet-} \rightarrow OH^\bullet + OH^- + O_2 \quad \ldots\ldots (6)$$

Equation (1) shows the initial photogeneration of excited electrons (e^-) and holes (h^+). Equations (2) and (3) show the hole oxidation reactions, while equations (4) and (5) represent the electron reduction reactions. The formed hydroxyl radicals ($OH^\bullet$) (equations 2 and 3) play an important role in starting oxidation reactions [56]. While the activity of superoxide radicals ($O_2^{\bullet-}$), produced from the reduction reaction of absorbed oxygen (O_2) as shown in equation (4), is considered an important factor to produce (H_2O_2) and singlet oxygen (O_2), which is represented in equation (5) [57]. Equation (6) shows the reduction of the H_2O_2 to form hydroxide ions and more hydroxyl radicals, as well as singlet oxygen is itself extremely reactive [58].

Chapter Three

Methodology

3.1 Introduction

In this chapter, the preparation process of TiO_2 nanoparticles will be described. The synthesis process of the sample was achieved using a microwave method. The basic principles of techniques that were used in this work to analyze the results will be clarified. Finally, the photocatalytic activity of the samples for degradation of the aqueous solution of methylene blue (MB) will be also explained.

3.2 Materials

All the materials utilized in the synthesis process were used without any purification. Titanium (IV) isopropoxide (TTIP, 98% Acros Organics) $Ti[OCH(CH_3)_2]_4$ was used as a TiO_2 precursor material. Two solvents were used to prepare the samples, Ethylene Glycol (EG, J.T. Baker 99.8% Anhydrous solvent) $C_2H_4(OH)_2$ and highly pure Deionized Water (DIW) H_2O, then controlled the condensation rates of TTIP. Ethanol (absolute J.T. Baker Reagent) C_2H_5OH and DIW H_2O were utilized to remove any residual organic species for the preparation process of the product. Methylene Blue (MB, 99% Merck Organics) $C_{16}H_{18}ClN_3S$ was used as a target pollutant in an aqueous solution.

3.3 Synthesis of TiO_2 Nanoparticles

Titanium dioxide (TiO_2) powder has been synthesized using the microwave method using Titanium (IV) isopropoxide (TTIP) as TiO_2 precursor material with Ethylene Glycol (EG) or with Deionized Water (DIW) as solvents and reducing agent for synthesis of submicrometer particles of the transitional metals.

In the Synthesis procedure, (10 ml) of TTIP was added dropwise into (100 ml) of EG or DIW in a glass vessel under vigorous magnetic stirring at 600 rpm for 10 min. The microwave-assisted synthesis was conducted using a home cooking microwave oven (QMO-62LS) as showed in figure (3.1), uses a 2.45 GHz microwave frequency for 5 min in (60%, 80% and 100%) of the maximum power (MP) (1200W) which are (720, 960 and 1200 W) respectively without stirring. When the titration process was achieved, the resulting solution was changed from a transparent color to a milky white, which indicates the formation of the TiO_2 nanoparticles (as shown in figure (3.2-a)).

Figure (3.1) The microwave oven.

The resulting precipitate was collected and washed with DIW and absolute ethanol several times to eliminate any residual organic species remaining in the final products under centrifugation at 4500 rpm for 5 min (the collected powder is shown in figure (3.2-b)). Then the product dried in an oven at a temperature of 60 ºC overnight. Finally, the powder was calcined at a temperature of 400 ºC in the air for 1h (the powder is shown in figure (3.2-c)), by using the furnace (ELF 11/14B) as shown in figure (3.3).

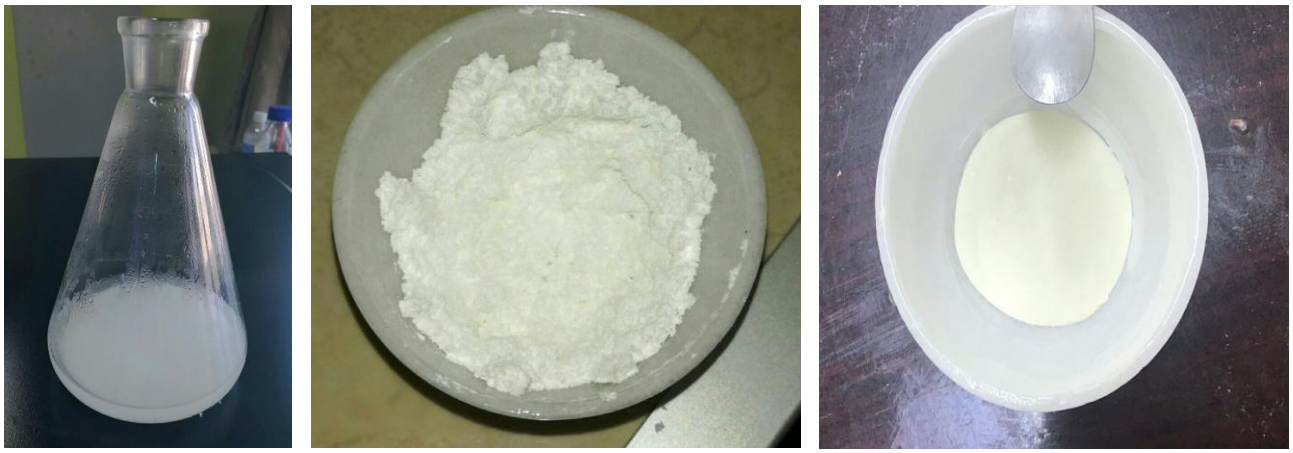

(a) **(b)** **(c)**

Figure (3.2) Steps of synthesize samples

(a) The milky white solution after the titration process.

(b) The collected powder after washing with ethanol and de-ionized water.

(c) the final product after annealing at 400 ºC for 1 h.

Figure (3.3) The Furnace (ELF 11/14B).

The schematic diagram for the whole preparation process of TiO_2 nanoparticles samples (EG60%, EG80% and EG100%), which was prepared in EG at power (60%, 80% and 100%) of maximum power respectively, and samples (DIW60% and DIW80%), which prepared in DIW at power (60% and 80%) of maximum power respectively, was shown in figure (3.4).

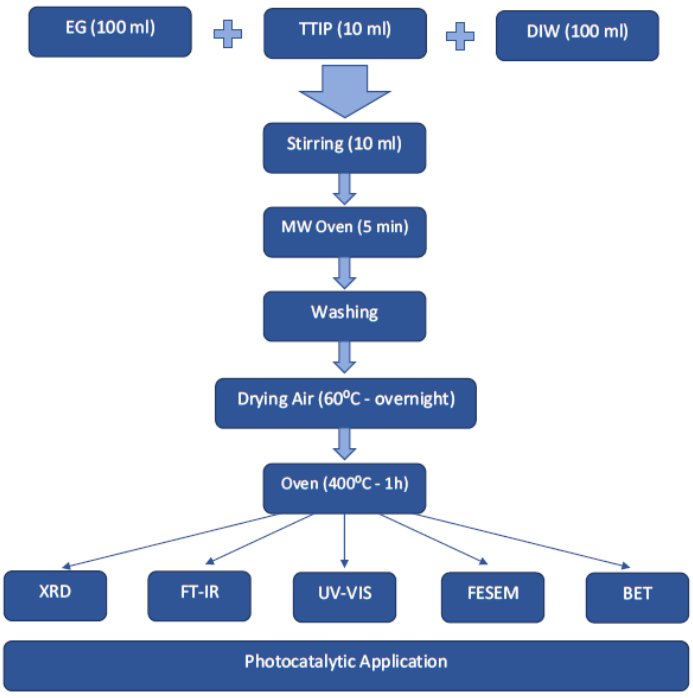

Figure (3.4) The schematic diagram for the preparation process of TiO_2 nanoparticles.

3.4 Characterization Techniques

TiO_2 Nanoparticles can be characterized by many types of equipment that are used to study the physicochemical and photocatalytic properties. This section describes the several characterization and analysis techniques utilized in this work.

3.4.1 X-Ray Diffraction (XRD) Analysis

X-Ray Diffraction is one of the important techniques used to characterize solid-state materials. It can provide valuable information about the lattice parameter, average crystallite size, phase structures, lattice strain, and the structure of the crystal patterns. In

this technique, the crystalline size that is measured is smaller than the measurement border of the electronic or optical microscope [59].

The principles of X-Ray Diffraction are simple. Monochromatic X-ray radiation is directed onto a crystal specimen, the constructional diffractions from parallel levels of atoms with space in between molecules (d) are obtained if Bragg's law is satisfied with the following equation:

$$2d \sin\theta = n\lambda \qquad \ldots\ldots (1)$$

The Scherrer equation can be used in the calculation of the crystal gain size in the shape of powder. EQ (2) shows how the Scherrer equation can be written [60].

$$D_{crys} = \frac{K\,\lambda}{\beta \cos\theta} \qquad \ldots\ldots (2)$$

Where θ is Bragg's angle, the wavelength by λ for the X-ray beam, and (n) is an integer that indicates the reflection order. If the wavelength of the X-ray beam is known, the interplanar spacing (d) can be obtained by measuring the Bragg angle θ. While K is a shape factor without dimension, D is the mean size of the regulated (crystal) fields, β is the line broadening at half the maximum intensity (FWHM).

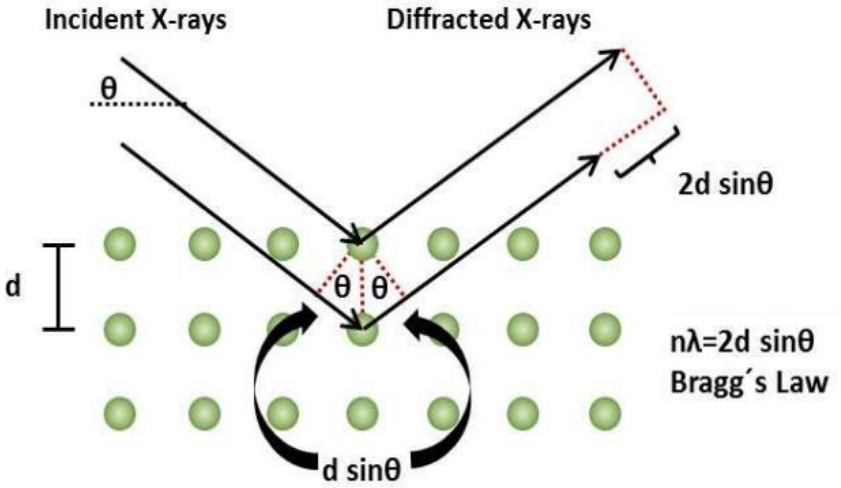

Figure (3.5) A schematic representation of the Bragg law [61].

The model of the used diffractometer was (6000 AS, 3K NOPC, Shimadzu-Japan) as shown in figure (3.6), which depends on Bragg's law (intensity as a function of the diffraction angle). The radiation source was CuKα1 at the wavelength (1.54056 Å) with operating conditions of the current (30 mA) and the voltage (40 kV). The test of the samples takes place for 2θ values between 10º and 80º with a step size of 0.020º and time exposed to radiation of about 15 sec per step. The prepared samples were examined in the School of Chemical Engineering University of Tehran - Iran.

Figure (3.6) The X-Ray Diffraction.

3.4.2 Specific Surface Area (BET)

Brunauer Emmett Teller (BET) is an essential method used to calculate the specific surface area and the distribution of pore size of different nanomaterials. The specified surface area of nanostructured materials is usually assigned by the physical absorption of inert gas molecules on the surface of the solid material by the BET process. The specific surface area of the prepared samples in this work was analyzed using micromeritics (Tristar II series) as shown in Figure (3.7). Typically, about (0.1 g) of each tested sample was weighed and placed in a specimen cell, which was volume calibrated. The sample was put into three stages, first, it was heated at a temperature that exceeded the maximum reasonable temperature for the specified material. Then, it was degassed at

120 ºC for 2 h under saturated vapour pressure (85.56 KPa) overnight by flowing an inert gas to remove any absorbent molecules. Finally, it was placed in a vacuum chamber that was cooled at a temperature of about -196 ºC (liquid nitrogen). The prepared samples were examined in School of Chemical Engineering University of Tehran – Iran.

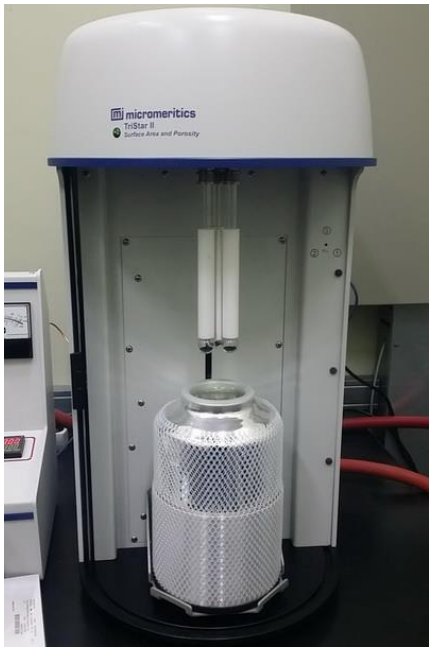

Figure (3.7) The micromeritics of analyzing the specific surface area.

The average pore diameter in addition to the pore volume of the sample was calculated by using Barrett-Joyner-Halenda (BJH) formula from N_2 (purity > 99.999%) adsorption-desorption isotherm. While the total specific surface area of the specimen can be assigned via the number of nitrogen molecules adsorption-desorption results with the variation of pressure [62]. There is a gradual increase then decrease in the relative pressure by using the accompanying software device. When the inert gas molecules come into contact with the surface of the solid, a number of inert gas molecules will be in desorption and absorption over a scope of the equivalent pressure, which define as an adsorption isotherm.

Whereas hand, according to IUPAC classification, there are various types of isotherms. These isotherms can be distinguished by several shapes, which are recognized

by the adsorbate or adsorbent types and the intermolecular interaction rate between the surface sample and gas [63, 64].

3.4.3 Field Emission Scanning Electron Microscopy (FESEM) and Energy Dispersive X-ray Spectroscopy (EDX)

The surface morphology characterization of TiO_2 nanoparticles samples was achieved by Field Emission Scanning Electron Microscopy (FESEM) (MIRA3 TESCAN - XMU) as shown in Figure (3.8). In FESEM, electrons are often used to screen the structure of a sample surface instead of light waves, the electron emitted (from an electron gun) is condensed by a series of electromagnetic lenses and directed on to the specimen surface. When the electron beam interacts with the specimen it produces several emissions of the electron from the specimen includes: (1) Secondary Electron (SE), (2) Backscattered Electrons (BSE), (3) Auger electrons, (4) X-Rays, and perhaps light. This interaction produces signals containing information about the surface morphology of the samples [65, 66]. The mechanism of an FESEM system is shown in Figure (3.9).

Figure (3.8) Field Emission Scanning Electron Microscopy.

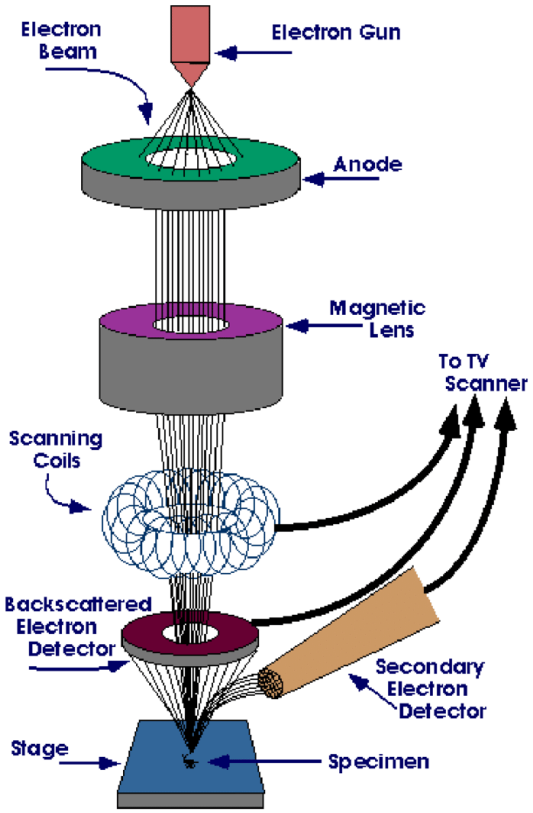

Figure (3.9) Schematic representation of the basic operation of a FESEM [67].

Generally, the difference between FESEM and SEM technique is that the spot size in FESEM is smaller than SEM, therefore it is possible to obtain images with very high magnification and low distortion [68]. This instrument can provide information on the constituent elements and compounds of the tested specimen by energy dispersive of X-Ray (EDX) spectroscopy. EDX relies on the detection of the sample through the interactions between the incident light beam and the specimen, where it is considered a special case of X-Ray analysis. While EDX provides characterization capabilities for each element of the sample and its quantity [69]. The prepared samples were examined in, School of Chemical Engineering University of Tehran - Iran.

3.4.4 Fourier Transform Infrared (FTIR)

Fourier transform infrared spectroscopy (FTIR) is a non-devastating technique that provides information about the particular effective groups in the organic as well as the inorganic materials such as polymers and metal oxides. The analysis of the sample is carried out using an infrared beam that passed during the sample and the absorption of radiation is calculated as a function of the frequency. FTIR spectrum shows the wavelength at which the specimen absorbs the infrared radiation. This allows the identification of the effective groups, chemical bonding, molecular structure, and the compounds in the sample [70].

FTIR is capable of causing a variety of vibrations and is determined by strict laws. IR spectroscopy energies were ranged between (4000-400) cm^{-1} and sometimes it extends to the far IR region of electromagnetic radiation. The obvious spectrum is usually obtained from pure samples with little IR active bonds while the complex sample structures give complicated infrared spectrum due to many absorption bands. The lattice vibrations of metal oxide were responsible for the absorption of active infrared bands. FTIR analysis is specific to the molecules that possess permanent dipole moments or phonons within the material having a crystalline structure.

In this study, the FTIR technique (Vectors 22, Brucker) as shown in Figure (3.10) with a single beam in the range between (4000-400) cm^{-1} was used to detect the chemical structure of samples. The instrument uses Michelson interference in spectrum analysis. The samples were measured by mixing KBr with TiO_2 nanoparticles as a pellet. The prepared samples were examined in School of Chemical Engineering, University of Tehran - Iran.

Figure (3.10) Fourier transform infrared spectroscopy device.

3.4.5 Ultraviolet-Visible Spectroscopy (UV-Vis)

Ultraviolet-Visible Spectroscopy (UV-Vis) measures the amount of absorption of spectroscopy within a specific region of ultraviolet and visible radiation. The spectrophotometer is composed of three parts: the light source, the dispersive, and the detector. A sample is put between a light source and a photodetector, where the strength of a UV-Vis light beam is measured before and after the sample passes through. UV-Vis absorption spectroscopy depends on the measurement of the percentage of absorbed radiation at each wavelength. Usually, it is performed by scanning the specimen via a range of wavelengths and recording absorption. This technique can be expanded to include solid and gaseous states as well as to measure the reflection and transition of light. The mathematical-physical principles for the measurements of the light absorption on the sample are formed by the Lambert-Beer law (equation 3). [71]

$$A = \log \frac{I_o}{I} = \frac{1}{T} = \alpha l c \qquad \ldots\ldots (3)$$

Where A is absorption, (α) is the absorptivity, (I_0) is the incident light intensity, (I) is the transmitted light intensity, T is the transmittance, (c) is the concentration of the sample, and (l) is the path length. Figure (3.11) illustrates Beer-Lambert law. [71].

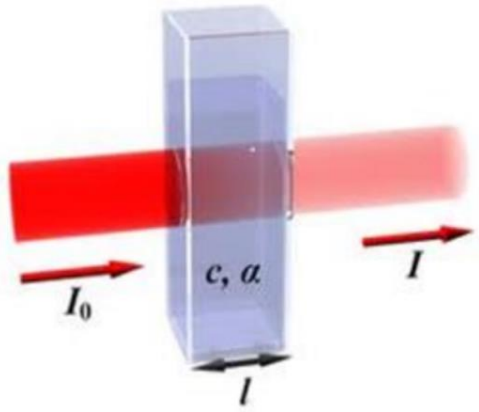

Figure (3.11) Beer-Lambert law [71].

Moreover, the semiconductor electronic bandgap can be measured using UV-Vis spectroscopy [72]. In this study, the UV-Vis spectrophotometer (T90+, PG instrument LTD) (shown in figure (3.12)) was used to monitor the degradation of methylene blue (MB) concentration during the assessment of photocatalytic activity via the prepared titanium dioxide (TiO_2) nanorods samples. The UV spectrum was recorded in the region between 190 and 1100 nm. The maximum absorption wavelength of MB (664 nm) was utilized to calculate the rate of degradation as a function of the time of irradiation. The prepared samples were examined in School of Chemical Engineering University of Tehran - Iran.

Figure (3.12) UV-Vis spectrophotometer device.

3.5 Photocatalytic Activity of TiO_2

3.5.1 Photodegradation Setup

The photocatalytic reactions were taking place in the metal frame (50 cm length × 30 cm width) that box was covered with aluminum foil. The reactor is horizontally fixed to the body of the frame. It consists of a quartz reactor (20 cm length × 4 cm diameter) with two outlets and a lamp (λ = 254 nm, 11 Watt) as a source of UV irradiation. The lamp is placed into the quartz reactor. One outlet is syringe to extract the sample and the other is a thermometer for control of solution temperature. In order to keep the solution cool and prevent the solution temperature from rising, cold water circulation was used by the cooler pump with a flow rate of one liter per minute (1 L/min). To homogenize the catalyst with the solution and prevent the catalyst from settling, the quartz reactor was placed on a stair heater. During the test, the front of the metal box was closed to prevent light loss and UV light hazards. The photodegradation setup is shown in figure (3.13).

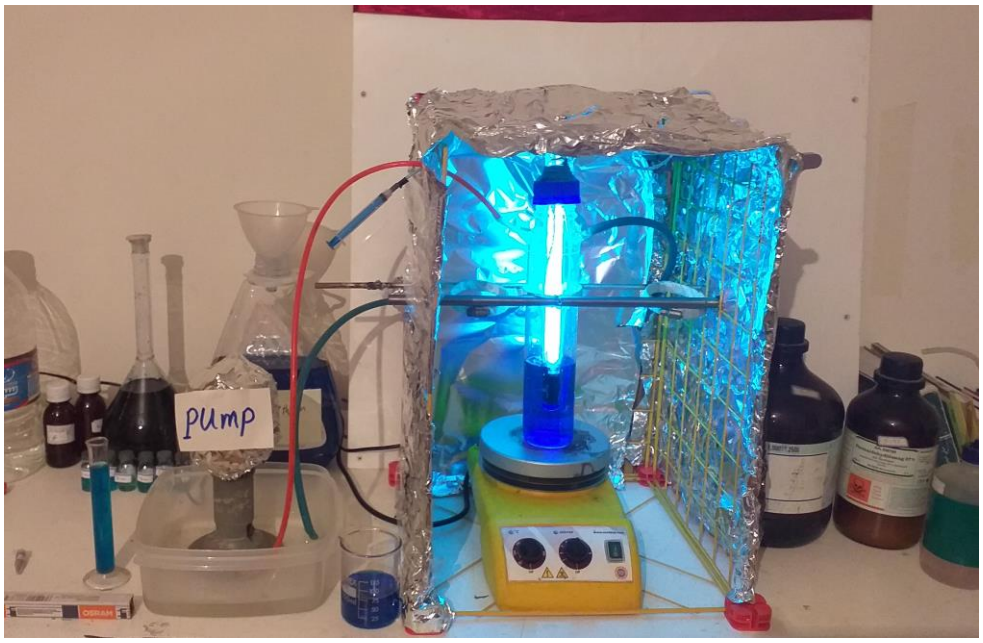

(a)

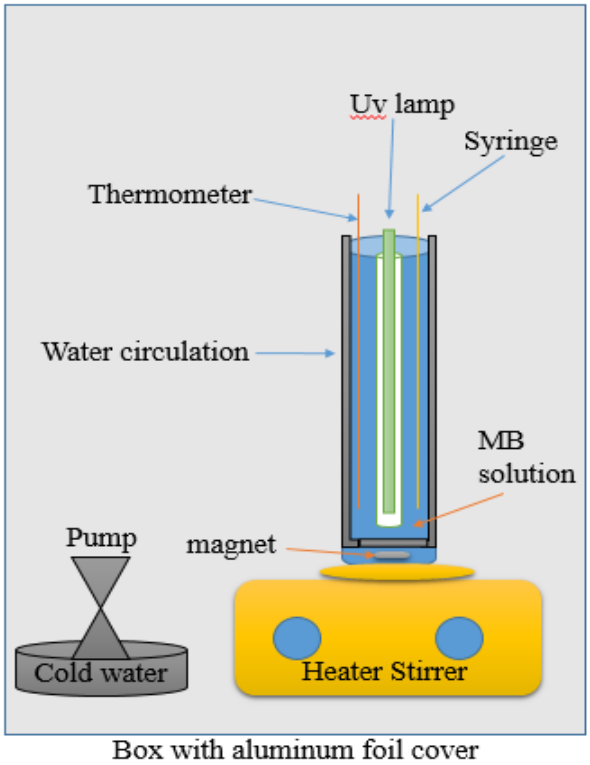

(b)

Figure (3.13) photographs of the (a) photocatalytic setup and (b) reactor parts.

3.5.2 Photocatalytic Studies

The photocatalytic activity of TiO_2 powder was tested using methylene blue (MB) solution as a model pollutant under ultraviolet (UV) light irradiation. Methylene blue is a shining-colored cationic dye with the molecular chemical formula $C_{16}H_{18}ClN_3S$. It was selected in this work due to its high absorbance to the surface of semiconductor metal oxide, higher resistance to degrading light, and clear optical absorption. The rate of degradation MB using the photocatalyst can be calculated from the variation in absorbance through the photodegradation process. The dye MB has extravagant absorption at the wavelength of about (664 nm) and the concentration of methylene blue can be assigned from the absorbance at this value of wavelength. The photocatalytic experiment was achieved at room temperature using TiO_2 nanoparticles as a catalyst.

Typically, the experiments were conducted as follows:

At first, a specific amount (100 mL) of methylene blue (MB) solution at a concentration of (10 ppm) was placed in a glass vessel. Then, (20 mg) of catalyst nanoparticle was added. In addition to the UV irradiation, to disperse the solid catalyst particles the suspension was sonicated for (10 min). Next, the solution was put in a darkroom to stir for at least 30 min to obtain the adsorption-desorption equilibrium of the dye MB on the catalyst surface and the elimination of any mistake caused by the elementary adsorption. The first sample (approximately 4 mL) was taken from the solution at the termination of the interval of the dark adsorption to determine the dye methylene blue concentration in the solution, which was considered as the primary concentration (C_o).

Then, the solution was placed in a plastic container inside the chamber setup under irradiation by UV lamp (wavelength 254 nm and intensity 11 Watt). Upon the irradiation, the samples, approximately 4 ml of the liquid, were drawn at a specific period of (20 min) and centrifuged immediately at (4500 rpm for 10 min) to remove any suspended solids. Finally, the clean solution was taken to determine the concentration of the MB in the solution using UV-Vis spectroscopy in the range (200-800) nm to monitor the methylene blue degradation.

The photodegradation rate for each sample was found to obey the first order kinetic model (pseudo). The MB degradation rate (k) was produced from the first order kinetic analyses according to the equation:

$$\ln (C_o/C_t) = kt \qquad \ldots\ldots (4)$$

where, C_o and C_t are the initial concentration of MB and the concentration at any time (t), respectively and k is pseudo (the first-order rate constant) per unit (min^{-1}). The rate constant for MB degradation (k) can be obtained from a plot of ln (C_o/C_t) versus the irradiation time (t). The percentage of photodegradation efficiency of prepared samples at selected temperatures has been calculated from the formula:

$$\text{Degradation efficiency (\%)} = \frac{C_o}{C_0 - C} \times 100\% \qquad \ldots\ldots (5)$$

where Co and C are the concentrations of the dye solution before and after ultraviolet (UV) irradiation [44].

Chapter Four

Results and Discussion

4.1 Introduction

In this chapter, characterizations of titanium oxide are presented and discussed by means of characterization studies (XRD, FESEM, EDX, BET and FTIR). In addition, the photocatalytic activity of TiO_2 nanoparticles prepared by microwave method at different microwave powers with two different solvents was studied with UV irradiation.

4.2 X-ray Diffraction Analysis

Figure (4.1) shows the X-ray diffractograms of the synthesized TiO_2 nanoparticles samples. From the X-ray patterns, eleven diffraction peaks were observed at 2θ = 25.28°, 37.85°, 48.05°, 53.89°, 55.06°,62.69°, 68.76°, 70.31°, 75.03°, 82.66° and 95.14°, which assigned to (101), (004), (200), (105), (211), (204), (116), (220), (215), (224) and (321) crystal lattice planes of TiO_2, respectively. These peaks have affirmed the formation of nanomaterials with high crystallization. It can be deduced that the TiO_2 nanoparticles synthesized in this work exist in the anatase TiO_2 phase (according to Joint Committee on Powder Diffraction Standard (JCPDS) file No. 021-1272). The formation of TiO_2 in the anatase phase is promising since numerous researchers reported that the anatase phase has high photocatalytic activity than other TiO_2 phases such as rutile and brookite [73]. The diffraction peaks of the prepared samples detect a sharp domain (101) peak at about 2θ=25.28º ascribed to a tetragonal structure of TiO_2 anatase phase with lattice constants a = b = 0.37852 nm, c = 0.65139 nm and angles $\alpha = \beta = \gamma = 90$. The X-ray patterns also showed that there are no peaks of other materials, indicating the samples were prepared with a high degree of purity.

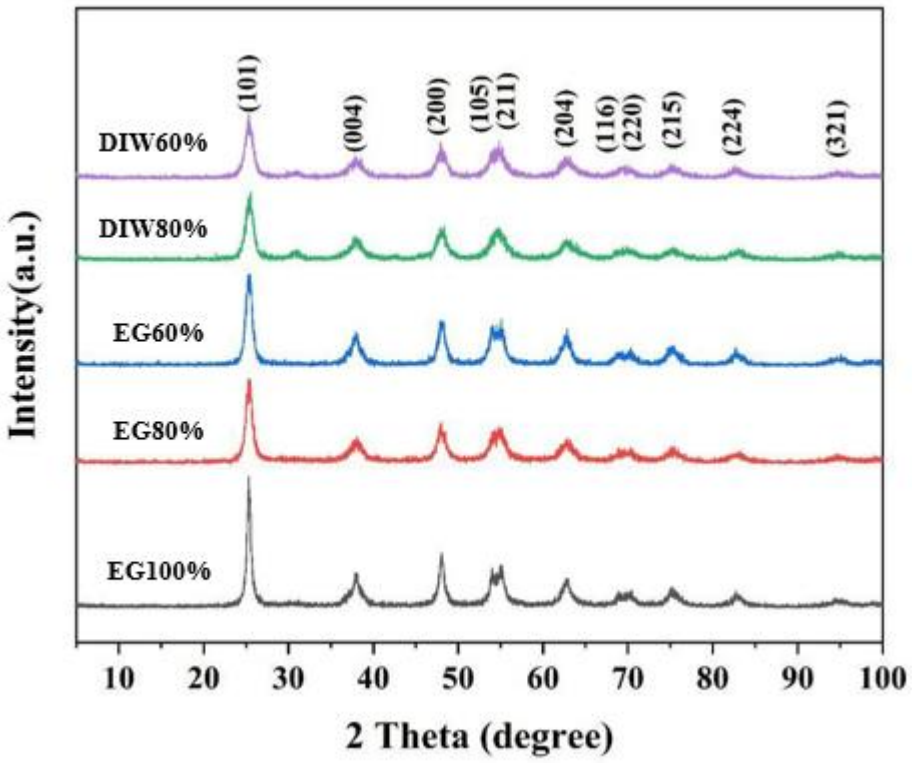

Figure (4.1) X-ray diffractograms of the TiO_2 nanoparticles.

Table (4.1) summarizes the XRD results for the prepared TiO_2 nanopowders. Therefore, the calcining temperature at 400 ºC for 1h was selected in this work to secure the TiO_2 anatase phase presence. The TiO_2 nanoparticles' average crystallite size calcined at this temperature has been determined from the broadening of anatase TiO_2 peaks at a difference of 2θ in the pattern using the Debye-Scherrer equation. Table (4.2) shows the average crystallite sizes of the samples (DIW60%, DIW80%, EG60%, EG80% and EG100%).

Table (4.1) XRD results for the prepared TiO_2 nanopowders.

Sample hkl	2θ ° standard	d-Spacing(Å) standard	2θ° DIW60%	d-Spacing(Å) DIW60%	2θ° DIW80%	d-Spacing(Å) DIW80%	2θ° EG60%	d-Spacing(Å) EG60%	2θ° EG80%	d-Spacing(Å) EG80%	2θ° EG100%	d-Spacing(Å) EG100%
(101)	25.28	3.52000	25.32	3.514702	25.54	3.484923	25.32	3.514702	25.32	3.514702	25.32	3.514702
(004)	37.85	2.37800	37.86	2.374444	37.86	2.374444	37.87	2.37384	37.86	2.374444	37.86	2.374444
(200)	48.05	1.89200	47.88	1.89832	48.10	1.89015	48.10	1.89015	47.89	1.897947	48.12	1.889412
(105)	53.89	1.69990	53.92	1.69906	53.92	1.69906	53.92	1.69906	53.92	1.69906	53.92	1.69906
(211)	55.06	1.66650	55.10	1.665432	55.10	1.665432	55.10	1.665432	55.10	1.665432	55.11	1.665154
(204)	62.69	1.48080	62.80	1.478476	62.79	1.478687	62.80	1.478476	62.80	1.478476	62.80	1.478476
(116)	68.76	1.36410	69.06	1.358943	68.60	1.366929	68.84	1.362748	68.58	1.367279	69.06	1.358943
(220)	70.31	1.33780	70.24	1.338975	69.99	1.343144	70.24	1.338975	70.32	1.337648	70.24	1.338975
(215)	75.03	1.26490	75.03	1.264925	75.03	1.264925	75.10	1.263919	75.10	1.263919	75.10	1.263919
(224)	82.66	1.16640	82.58	1.16735	82.80	1.164806	82.58	1.16735	82.80	1.164806	82.80	1.164806
(321)	95.14	1.04360	94.92	1.045459	95.14	1.043622	94.92	1.045459	94.92	1.045459	95.14	1.043622

Table (4.2) The average crystallite sizes of the prepared TiO_2 nanoparticles.

Sample	Average crystallite size (D) (nm)
DIW60%	5.28
DIW80%	4.78
EG60%	6.47
EG80%	5.50
EG100%	8.33

4.3 Specific Surface Area (BET) Results

The typical isotherm nitrogen (N_2) adsorption and desorption of anatase TiO_2 nanoparticles are shown in figure (4.2) for (EG60%, EG80% and EG100%) samples, and in figure (4.3) for (DIW60% and DIW80%) samples. The irregular distribution of pores size of the TiO_2 nanoparticles samples resulted in a hysteresis loop between the two curves (adsorption and desorption) [74]. The hysteresis's loop shape is essential to provide other details of the nanostructure of the prepared samples.

A gradual change in the adsorption-desorption branch under a substantial range of pressure (P/P_0) is shown in the isotherm of the synthesized samples, which indicates a mesoporous material is present. According to the (International Union of Pure and Applied Chemistry) (IUPAC) classification, the prepared samples show the type IV isotherm [75].

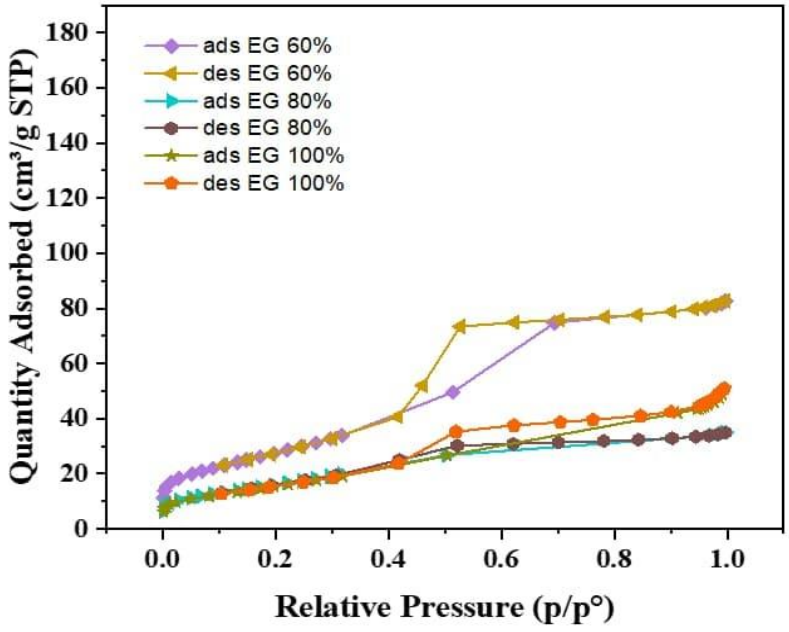

Figure (4.2) (N_2) adsorption-desorption of anatase TiO_2 nanoparticles for (EG60%, EG80%, and EG100%) samples.

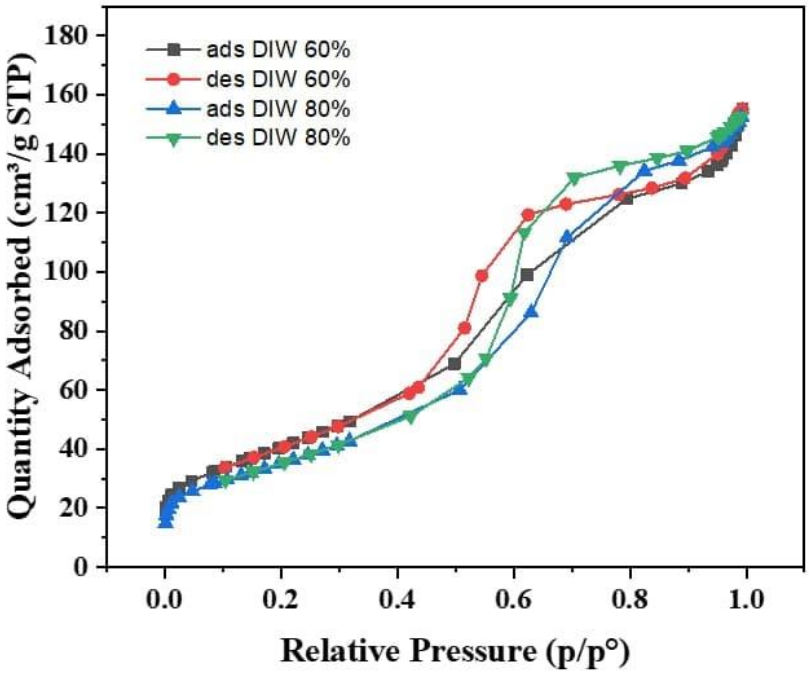

Figure (4.3) (N_2) adsorption-desorption of anatase TiO_2 nanoparticles for (DIW60% and DIW80%) samples.

The adsorption-desorption isotherm for the TiO_2 nanoparticles can be divided into four regions as shown in figure (4.4). The first region is at a relative pressure (P/P_0) below (0.3), the isotherm shows a gradual increase of adsorption, which indicates that the samples have micropores with a size below (2 nm). At the second region, the relative pressure is between (0.3 and 0.42), the isotherm shows weak hysteresis loops indicating that the samples contain mesopores with a size between (2 nm and 50 nm) [76]. In the third region when the relative pressure is between (0.42 and 0.7), the isotherm reveals a distinct capillary concentration [77]. Finally, in the fourth region, with the highest relative pressure above (0.7), a small hysteresis loop can be observed indicating the existence of larger mesopores [78].

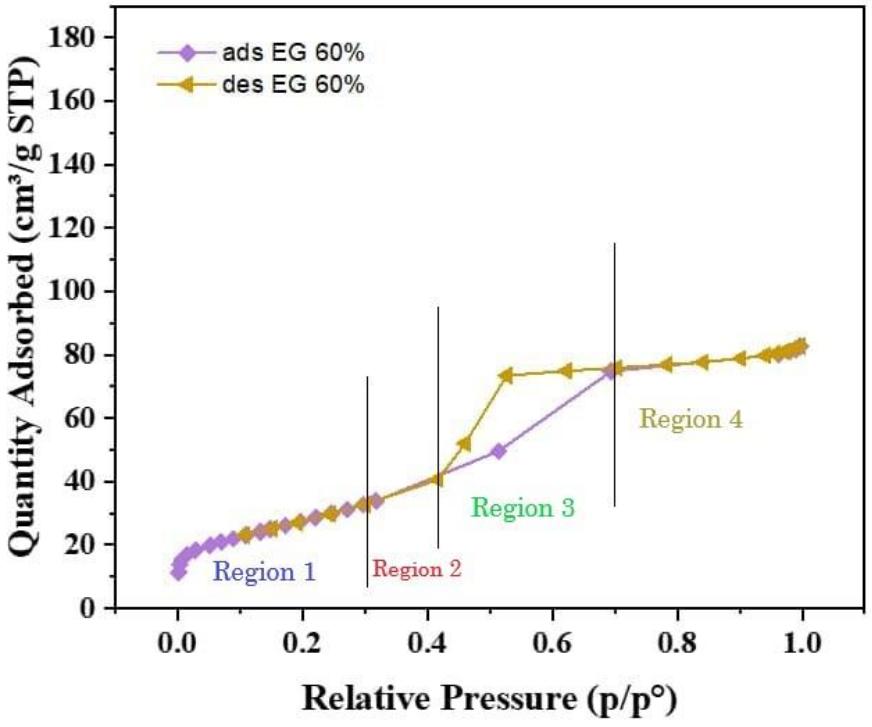

Figure (4.4) The typical N_2 adsorption-desorption isotherm of anatase TiO_2 nanoparticles for (EG60%) sample.

The specific surface area of the synthesized TiO_2 nanoparticles was approximately found to be (103.36, 60.74, 58.75, 151.41 and 130.76) $m^2\ g^{-1}$, for the samples (EG60%, EG80%, EG100%, DIW60% and DIW80%) respectively. The results in this work were greater than the TiO_2 nanoparticles previously reported (87 $m^2\ g^{-1}$) [35], (95 $m^2\ g^{-1}$) [32]. This observation could be due to the wider and broader distribution of space among particles in the spherical structure in the samples (DIW60% and DIW80%) [79], and to the one-dimensional nanorods in the samples (EG60%, EG80% and EG100%), as shown in FESEM images.

Using the Barret-Joyner-Halenda (BJH) method, the distribution pattern of the pore size was evaluated from the N_2 isotherm desorption branch [80], as shown in figures (4.5, 4.6). The results show that the average pore size of the prepared samples is about (3.77, 3.23, 4.25, 4.94, 5.3) nm and the average pore volume is about (0.131, 0.057, 0.0777, 0.246, 0.24) cm^3g^{-1} for the samples (EG60%, EG80%, EG100%, DIW60% and DIW80%) respectively.

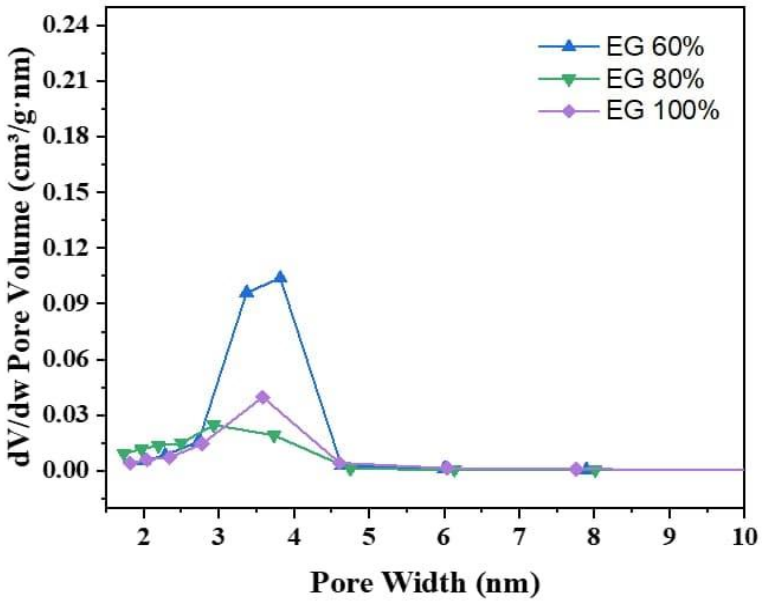

Figure (4.5) Pore size distribution of anatase TiO_2 nanoparticles for (EG60%, EG80% and EG100%) samples.

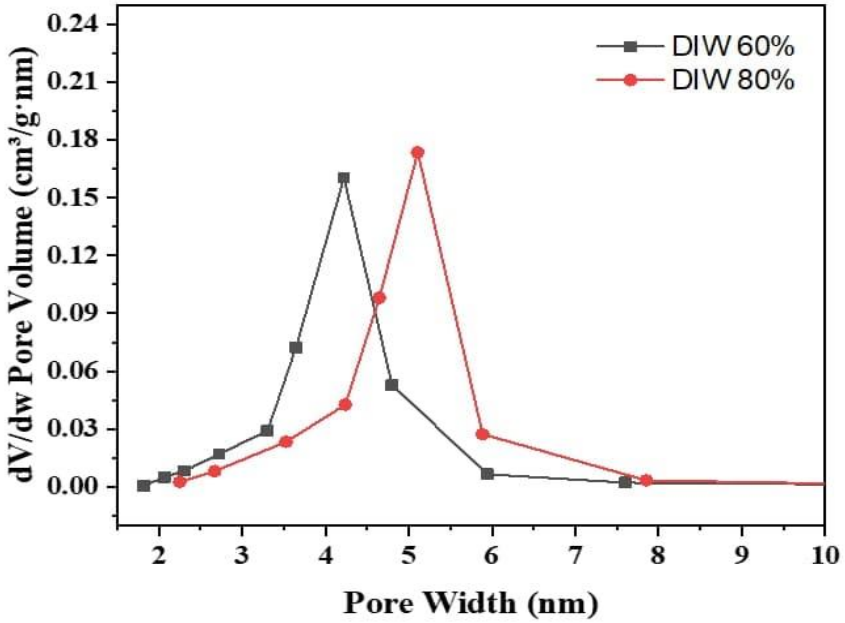

Figure (4.6) Pore size distribution of anatase TiO_2 nanoparticles for (DIW60% and DIW80%) samples.

Table (4.3) shows the specific surface area, the average pore size and pore volume of the prepared TiO_2 nanoparticles samples.

Sample	Specific surface area (m^2 g^{-1})	Pore size (nm)	Pore volume (cm^3g^{-1})
EG60%	103.36	3.77	0.131
EG80%	60,74	3.23	0.057
EG100%	58.75	4.25	0.079
DIW60%	151.41	4.94	0.25
DIW80%	130.76	5.3	0.24

It can be noticed that the samples (DIW60% and DIW80%) have a higher surface area than the samples (EG60%, EG80% and EG100%) due to the high pore volume of the DIW samples. Generally, the increase in the surface area of the catalytic nanomaterial may cause an increase in the photocatalytic activity. The large surface area provides extra active positions to absorb the polluted methylene blue (MB) solution.

4.4 FESEM and EDX Results

Figures (4.7 - 4.11) show the surface morphology of prepared samples after annealing at a specific temperature which was investigated using field emission scanning electron microscopy (FESEM).

The images of (FESEM) for EG60%, EG80% and EG100% samples in figures (4.7 - 4.9) show that uniform rod-like shapes of TiO_2 nanoparticles were conglomerated successfully with distinct sizes via this process. The results show the size of the nanoparticles started to grow with increasing the preparation power from 60%, 80%, to 100% from the maximum Microwave Power (MP) (1200W). There is no growth of the TiO_2 nanorods that took place at a power of preparation less than (60%MP) for the Ethylene Glycol samples. While at the preparation power (50%MP), the TiO_2 nanoparticles do not form due to the titanium glycolate complex was too stable to decompose and higher temperatures (produced by higher powers) increased the rate of growth. The FESEM images of samples EG60%, EG80% and EG100% showed the formation of TiO_2 nanorods with flat and straight faces.

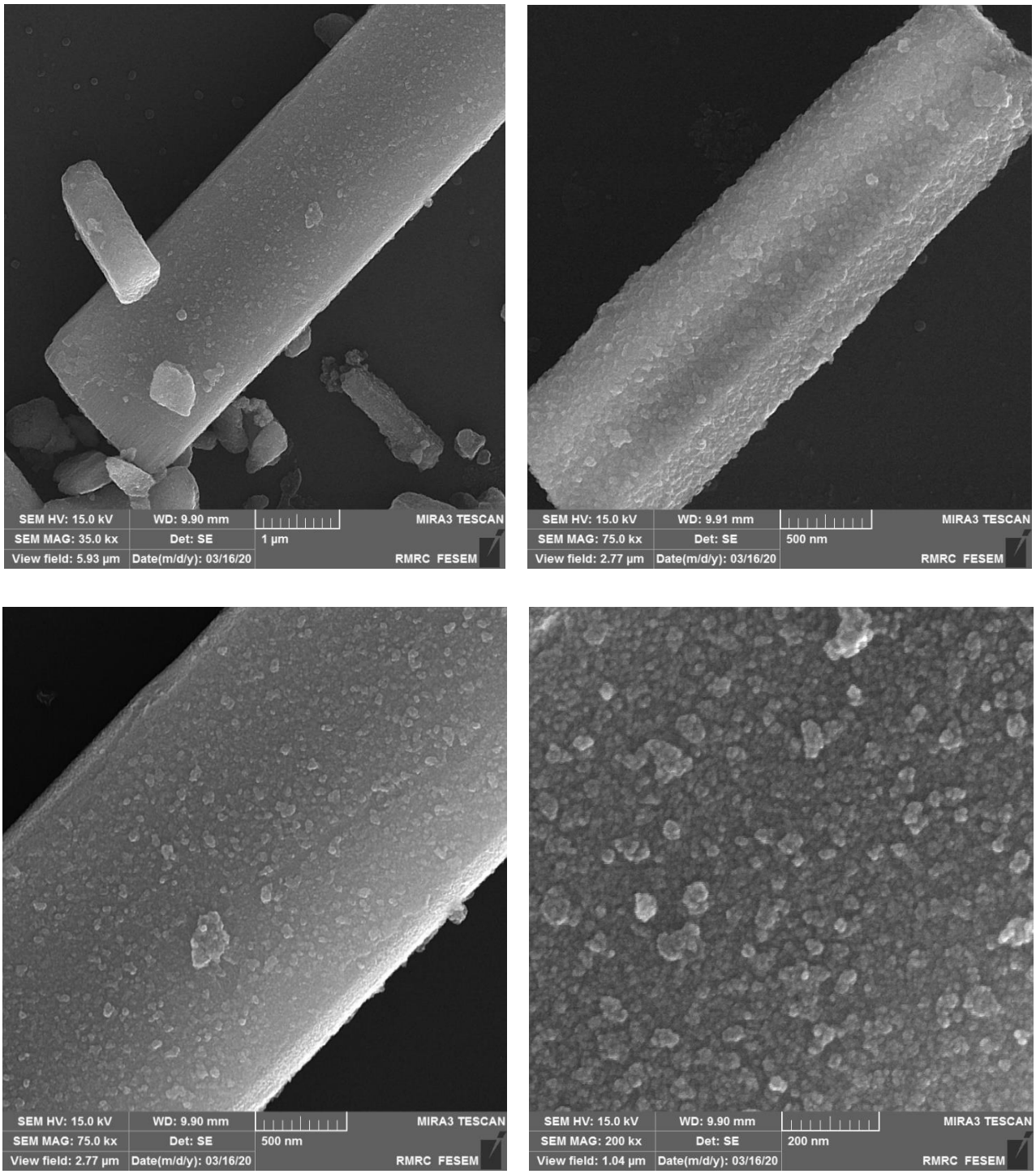

Figure (4.7) FESEM images of TiO_2 nanoparticles for EG60% sample.

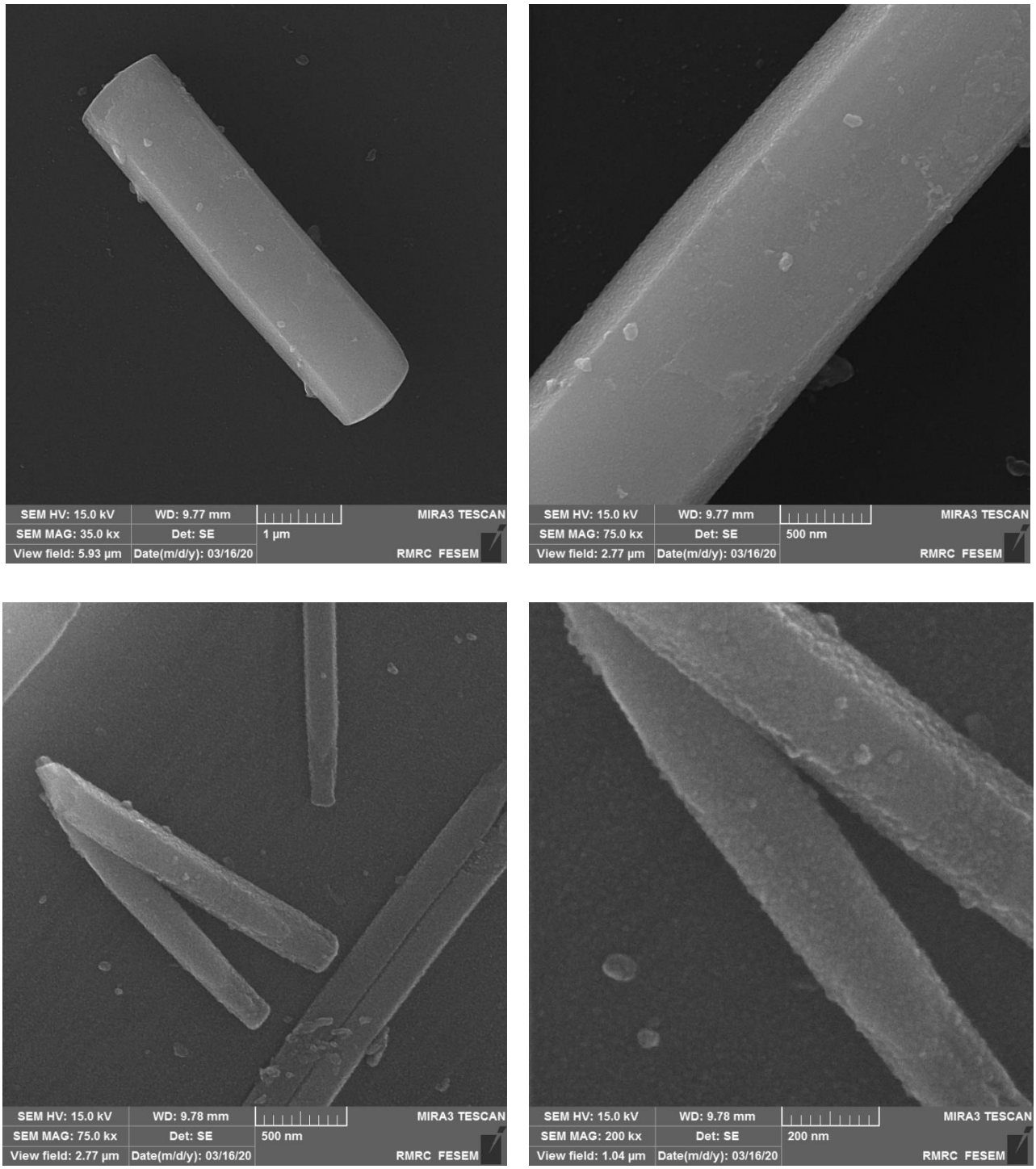

Figure (4.8) FESEM images of TiO_2 nanoparticles for EG80% sample.

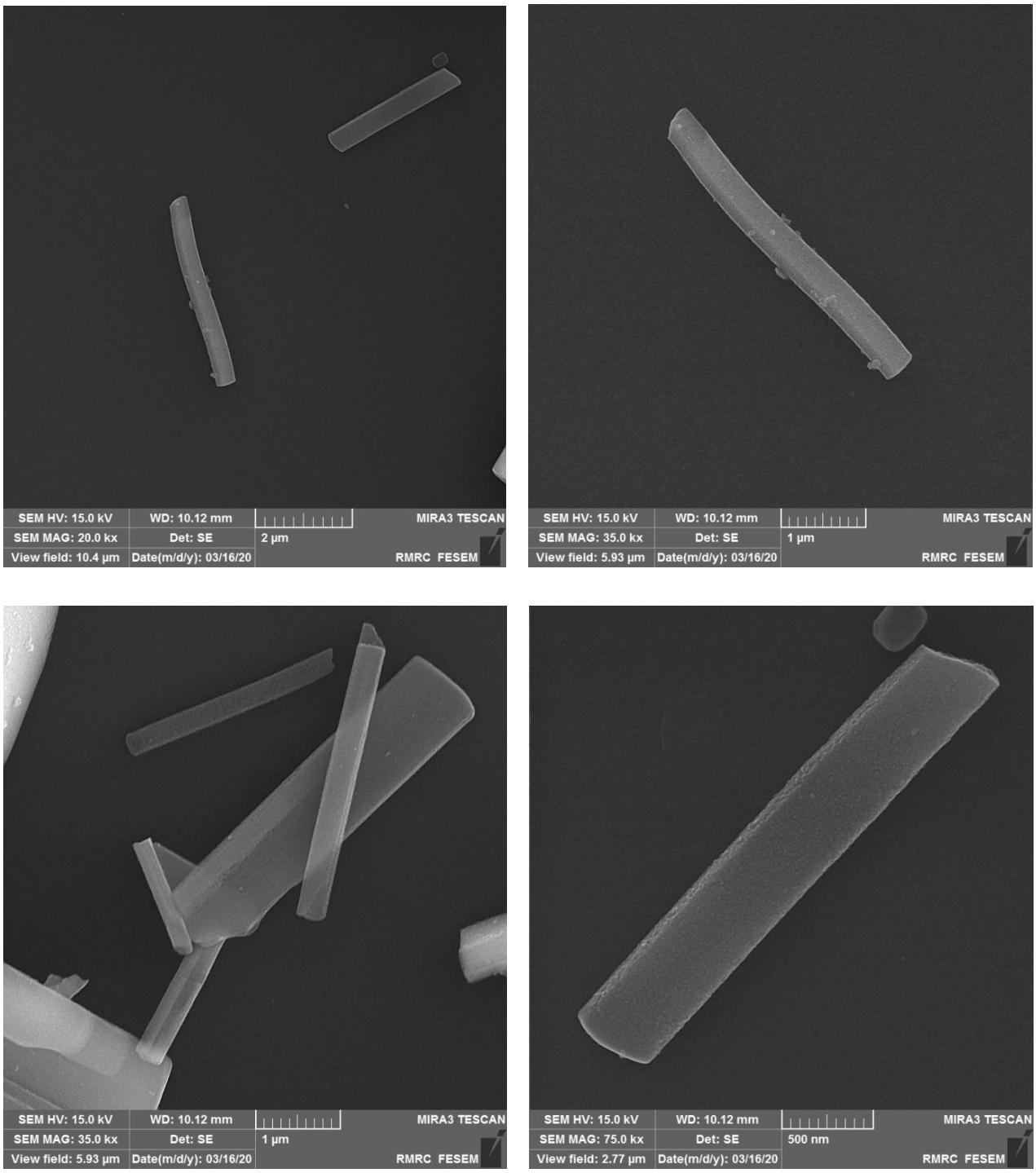

Figure (4.9) FESEM images of TiO_2 nanoparticles for EG100% sample.

The lengths of these nanorods were regular with an average of about (650, 2200 and 2800) nm and average particle width (diameter) about (140, 183 and 313) nm for the samples (EG60%, EG80% and EG100%) respectively. TiO_2 nanorods became longer, distinguishable and much thinner when the power increased. Table (4.4) summarizes the average lengths, diameters, and aspect ratio of TiO_2 nanorods synthesized at the selected powers.

Table (4.4) The average lengths, diameters, and aspect ratio of TiO_2 nanorods.

Sample	Average length (nm)	Average diameter (nm)	Aspect ratio (length/diameter)
EG60%	650	140	4.64
EG80%	2200	183	12
EG100%	2800	313	8.94

For the samples DIW60% and DIW80%, the FESEM images in figures (4.10, 4.11) show that the structure of the samples has a non-uniform distribution of spherical particles and they consist of either some single particles or cluster of particles with an average size of (15.33 and 12.83) nm diameter for the samples DIW60% and DIW80% respectively. A closer view of the FESEM images showed rough surface and high pore size which caused high specific surface areas for the samples DIW60% and DIW80% compared with EG60% EG80% and EG100% samples. Also, it can be observed that in the EG samples, the EG60% has a higher pore volume compared with the EG80% and EG100%, due to its slightly rough surface, this observation is in good agreement with the BET results. Generally, it was concluded that there is a proportional relationship between the microwave power and the particle size.

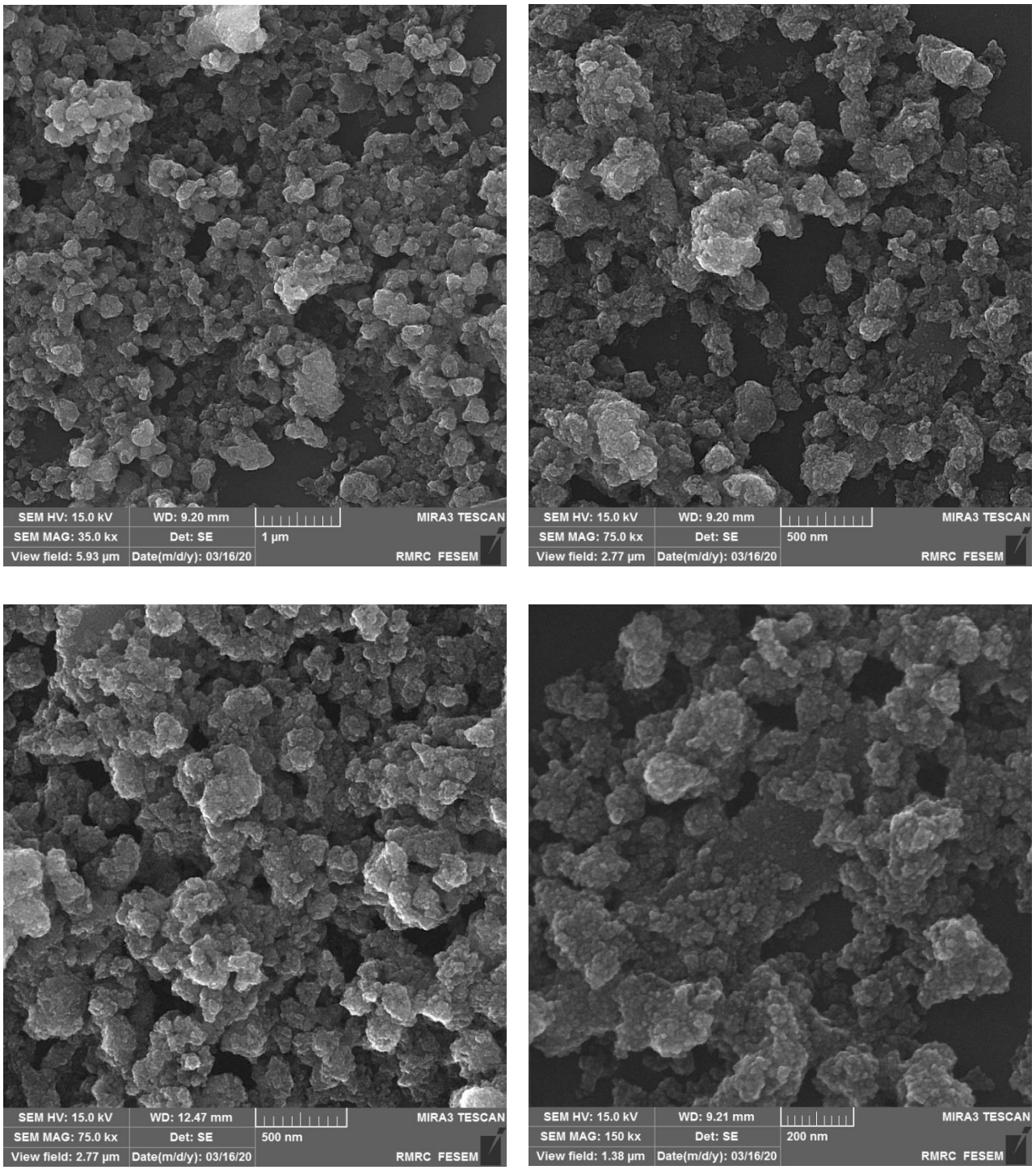

Figure (4.10) FESEM images of TiO_2 nanoparticles for DIW60% sample.

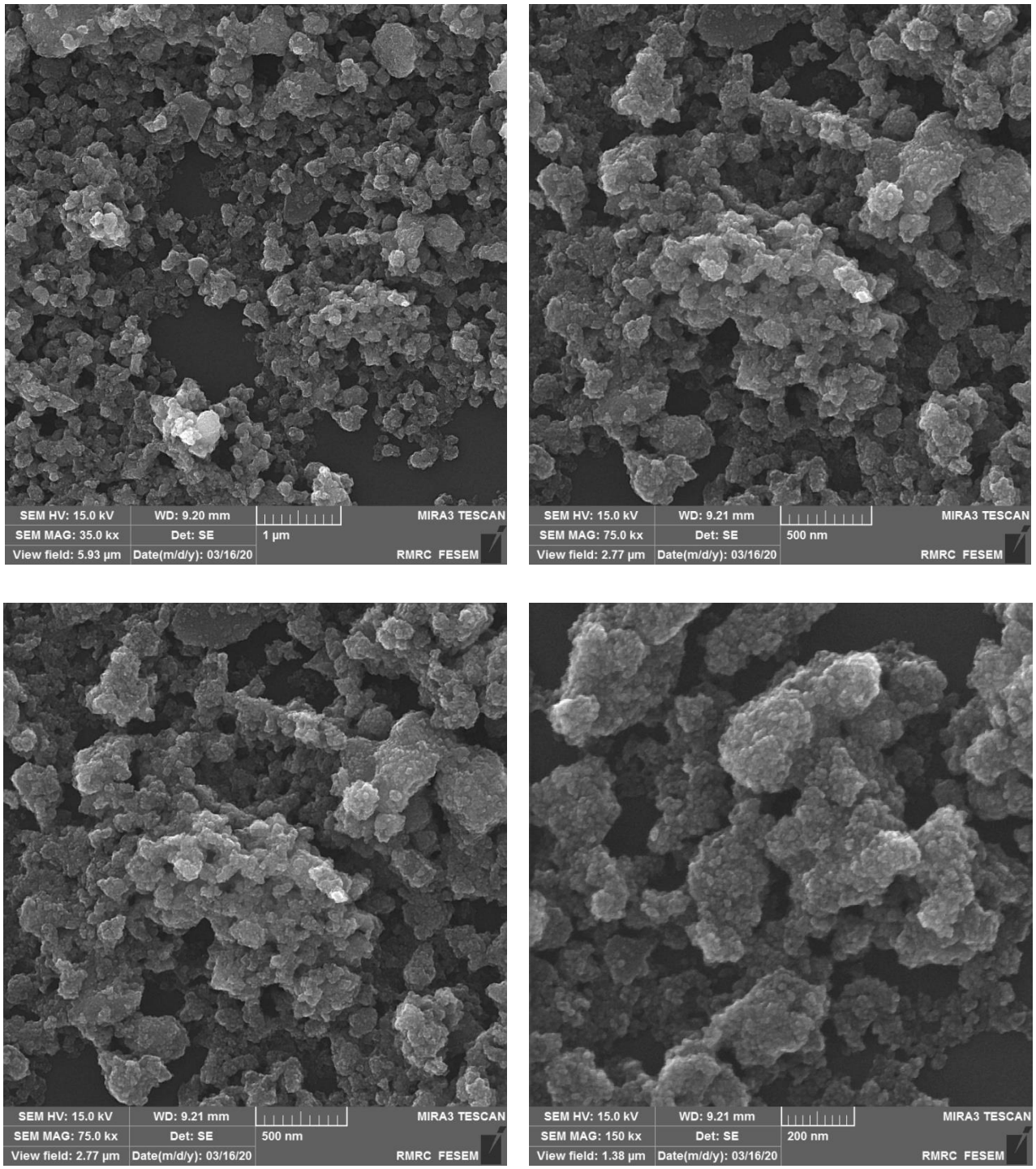

Figure (4.11) FESEM images of TiO_2 nanoparticles for DIW80% sample.

Figures (4.12 – 4.16) represent EDX spectra of TiO_2 nanoparticles for (EG60%, EG80%, EG100%, DIW60% and DIW80%) samples. The EDX analysis affirmed the atomic composition of the prepared samples. The results show that the spectra consisted of titanium (Ti) and oxygen (O) peaks with high intensity indicating the successful synthesis of pure TiO_2 nanoparticles. From EDX analysis, the elemental percentages of Ti were found to be (30.49%, 25.97%, 22.57%, 24.44% and 21.44%), while elemental percentages of oxygen (O) were found to be (69.51%, 74.03%, 77.43%, 75.56% and 78.73%) in the prepared samples (EG60%, EG80%, EG100%, DIW60% and DIW80%), respectively. The quantitative details about the EDX analysis are listed in the table (4.5).

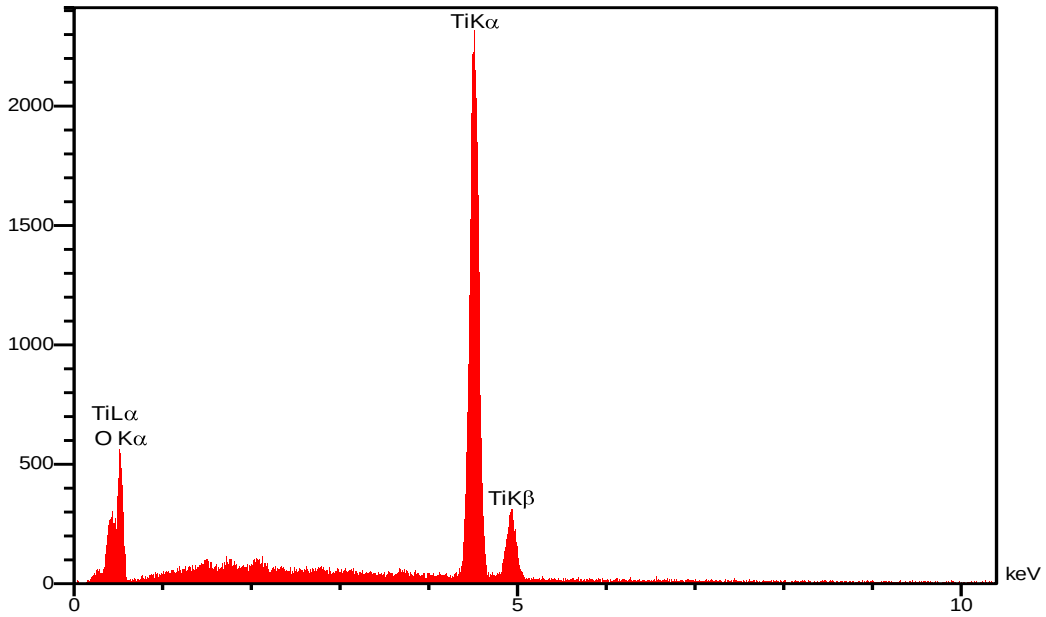

Figure (4.12) EDX spectrum of TiO_2 nanoparticles for EG60% sample.

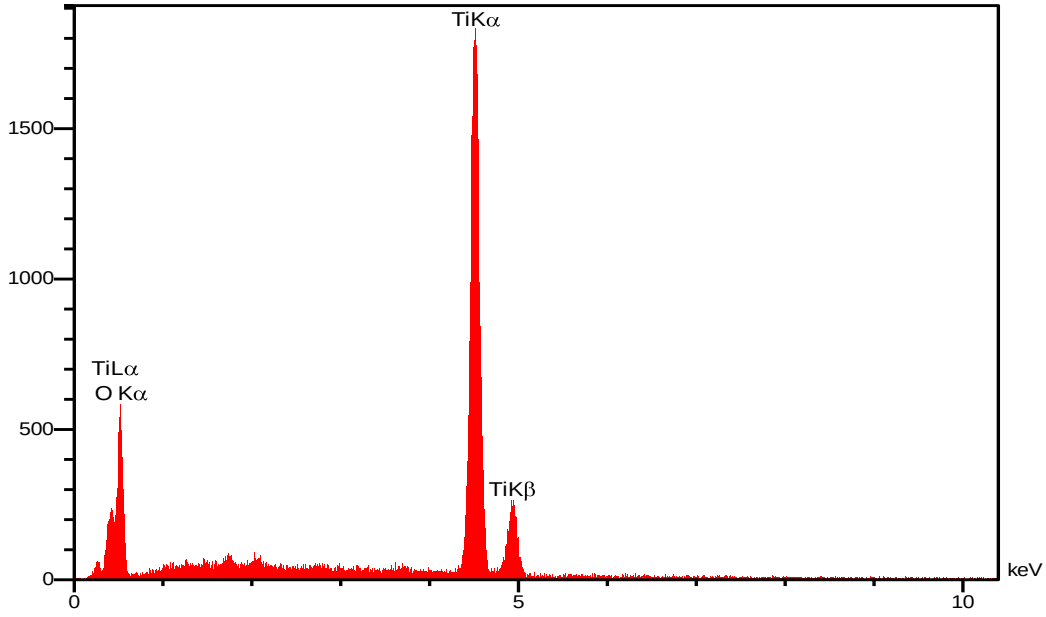

Figure (4.13) EDX spectrum of TiO_2 nanoparticles for EG80% sample.

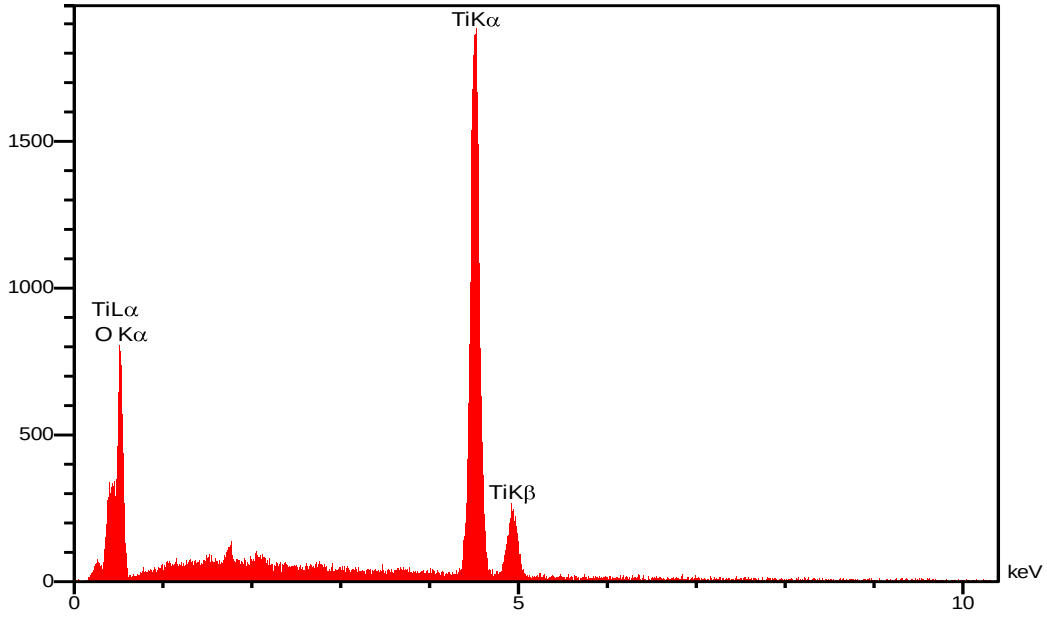

Figure (4.14) EDX spectrum of TiO_2 nanoparticles for EG100% sample.

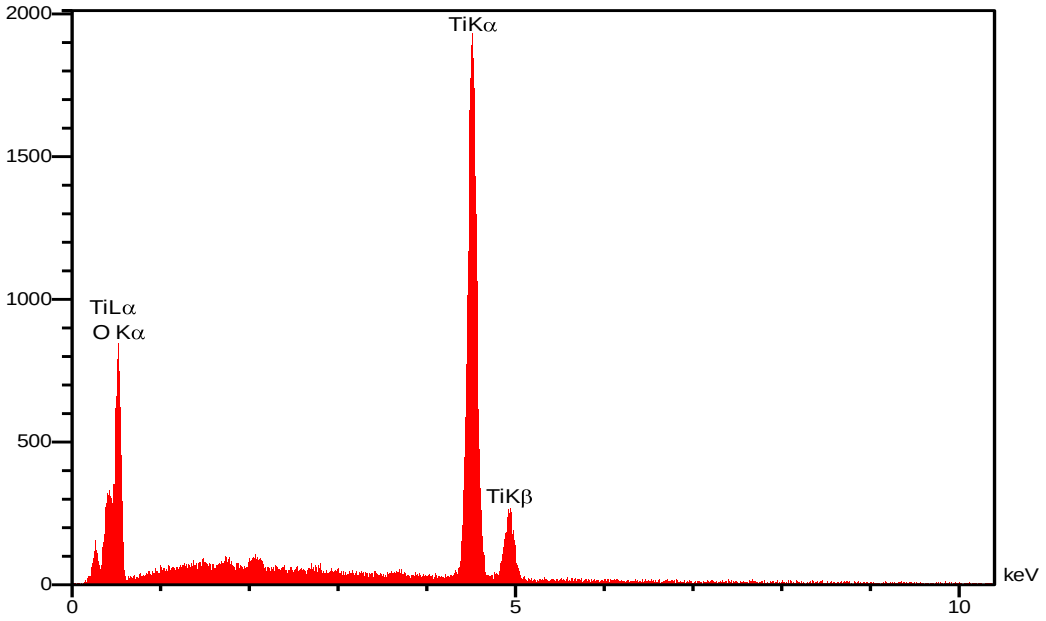

Figure (4.15) EDX spectrum of TiO_2 nanoparticles for DIW60% sample.

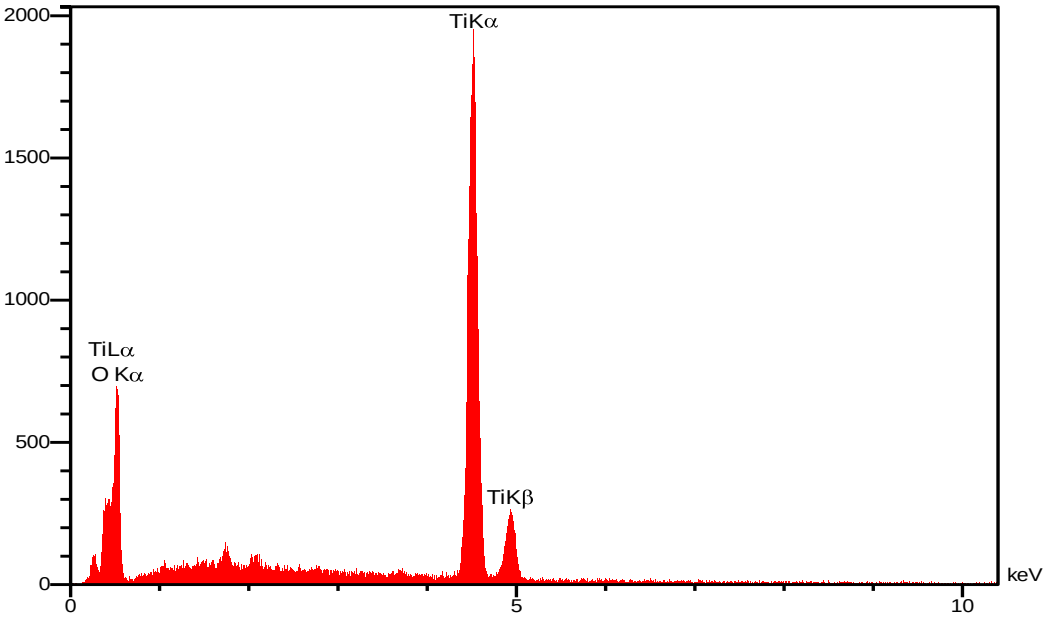

Figure (4.16) EDX spectrum of TiO_2 nanoparticles for DIW80% sample.

Table (4.5) the quantitative details about the EDX analysis.

Sample	Oxygen elemental percentage (at %)	Titanium elemental percentage (at %)	Total %
EG60%	69.51	30.49	100
EG80%	74.03	25.97	100
EG100%	77.43	22.57	100
DIW60%	75.56	24.44	100
DIW80%	78.73	21.44	100

4.5 FTIR Results

Figure (4.17) shows the FTIR spectrum recorded from the prepared TiO_2 nanoparticles and summarized in table (4.6). The broad and absorption band at (3300 - 3700) cm^{-1}, was related to the stretching vibration of hydroxyl O-H group at (3394.1 - 3444.24) cm^{-1}, which is due to the physical absorption of water, indicating the presence of moisture in the samples [81, 82]. The two absorption bands were attributed to the symmetric and asymmetric C-H stretching vibrations to the hydrocarbon groups of residual organic species, which was not completely removed by ethanol and distilled water washing [81]. The peak at 2854 cm^{-1} was attributed to the asymmetric CH_2 groups of the hydrocarbon moiety. Therefore, the peak 2923.55cm^{-1} can be indicated to the asymmetric stretching of -CH_3 terminal groups of the alkyl chain [83]. While the band at 2360.44 cm^{-1} was attributed to the O-H bending vibrations of interacting of the group's hydroxyl - included hydrogen bonds - with asymmetric and symmetric OH modes of the water molecules [84]. The weak band occurs at 1627.62 cm^{-1} assigned to O-H bending groups due to chemically absorbed water in solution [81]. While the presence of another peak at approximately 1523.48 cm^{-1} was characterized as the bending of CH_2 groups [82]. At approximately 1400 cm^{-1}, the peak was attributed to the carboxyl (C=O) and methylene groups stretching vibrations for ethylene glycol (EG) or might also be resulted

from residual organic species [81, 82]. The peaks appeared between ~ 470 cm^{-1} and 748 cm^{-1}, that was attributed Ti-O-Ti stretching vibrations in the anatase phase, which signified broad absorbance of titanium dioxide due to bending vibration of Ti-O stretching turned into Ti-O-Ti bridge stretching [84].

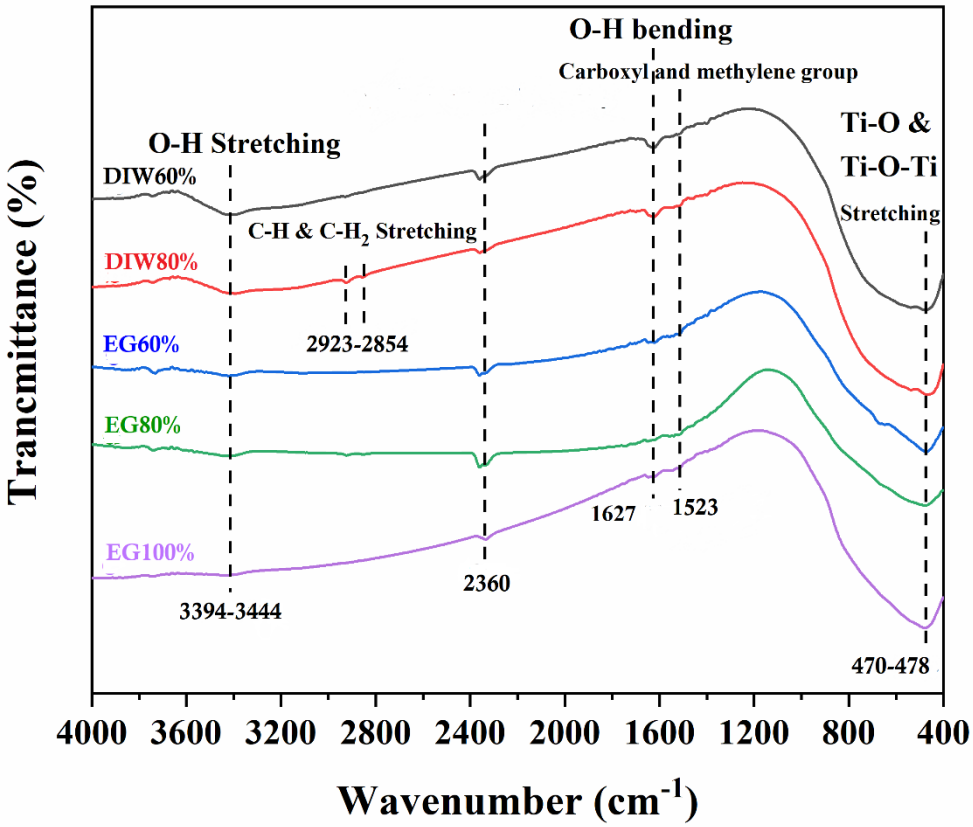

Figure (4.17) FTIR spectrum of the prepared TiO_2 nanoparticles.

Table (4.6) summarize the FTIR spectrum of the prepared TiO_2 nanoparticles.

Assignments	Wavenumbers (cm^{-1})
O – H stretching	3394.1- 3440.38
C – H stretching	2923.55 - 2854.13
O – H bending	2360.44
O – H bending	1627.62
C – H bending	1523.48
C = O stretching	1400
Ti-O-Ti stretching	721 – 748
Anatase TiO_2	470 – 478

4.6 Photocatalytic Results

The photocatalytic studies of the synthesized TiO_2 nanoparticles were carried out on the degradation of the methylene blue (MB) as an organic pollutant under ultraviolet (UV) irradiation for a certain duration. All the photocatalytic reactions of the samples have occurred in the air, through the oxidation process of MB aqueous solution.

Figure (4.18) shows the UV-Vis absorption spectra of MB solution without UV irradiation in the presence of the TiO_2 nanoparticles sample. From the figure, no degradation of MB dye solution without UV irradiation was observed in this experiment. The slight decrease in the spectra of absorbance was recorded due to the absorption of MB dye on the surface of the TiO_2 nanoparticles sample.

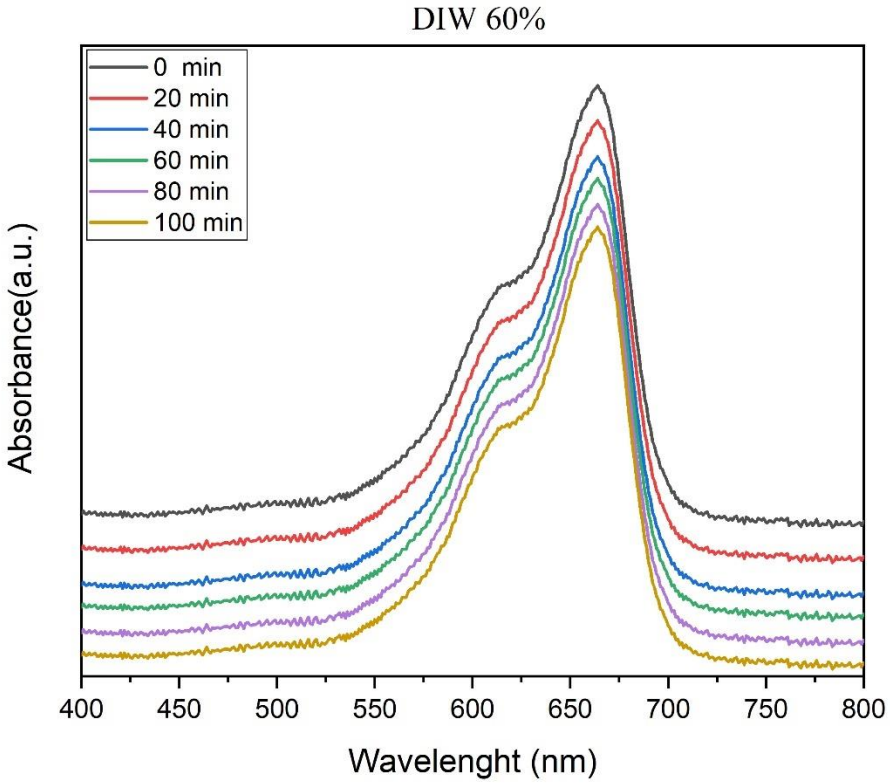

Figure (4.18) Absorbance spectra of MB versus wavelength without UV irradiation in the presence of the TiO_2 nanoparticles for DIW 60% sample.

The decrease in the maximum absorption peaks was obviously observed in the presence of UV irradiation, which can be attributed to the vigorous interactions between the TiO_2 nanoparticles surface and MB dye solution under irradiation. Moreover, it can be concluded that the absorption peak for the MB has been distinguished at the wavelength of (664 nm). The wavelength was determined from the corresponding value of the highest point in the absorption spectra of the MB solution. This value was in agreement with the standard wavelength of methylene blue dye [85].

The variation in the max absorption spectra of the MB at the wavelength (664 nm) irradiation with TiO_2 samples is shown in figures (4.19 - 4.23). All the data in the figures indicated that as the irradiation duration was increased, the intensities of the absorption peaks of spectra decreased. The peaks become weaker after a duration of 100 min of UV irradiation, which indicated the degradation of MB solution. Due to the oxidation and reduction process of the electron-hole pairs to the MB molecules.

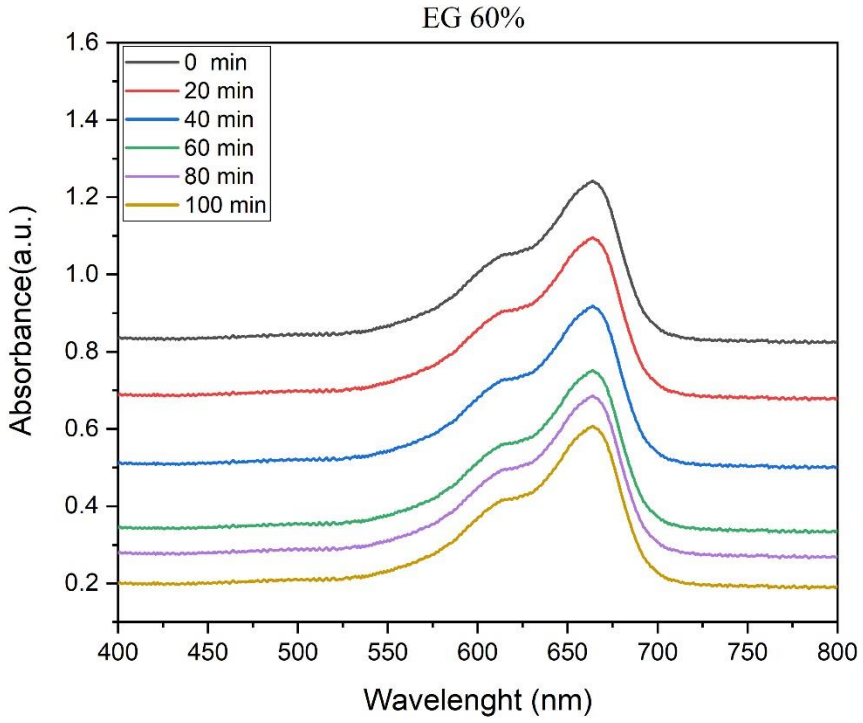

Figure (4.19) MB solution UV-Vis absorption spectra after photocatalysis for EG60% sample with different reaction times.

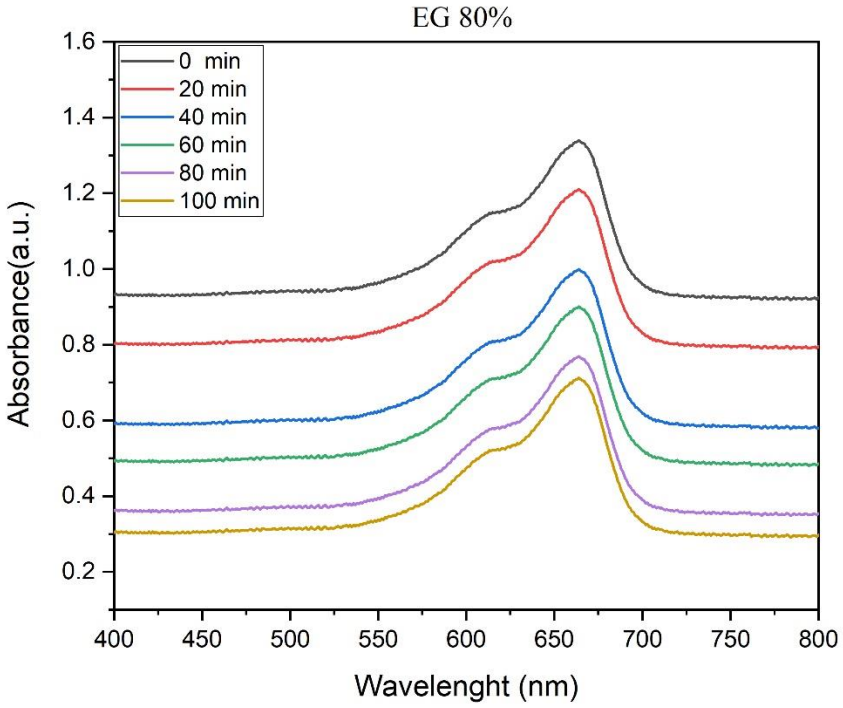

Figure (4.20) MB solution UV-Vis absorption spectra after photocatalysis for EG80% sample with different reaction times.

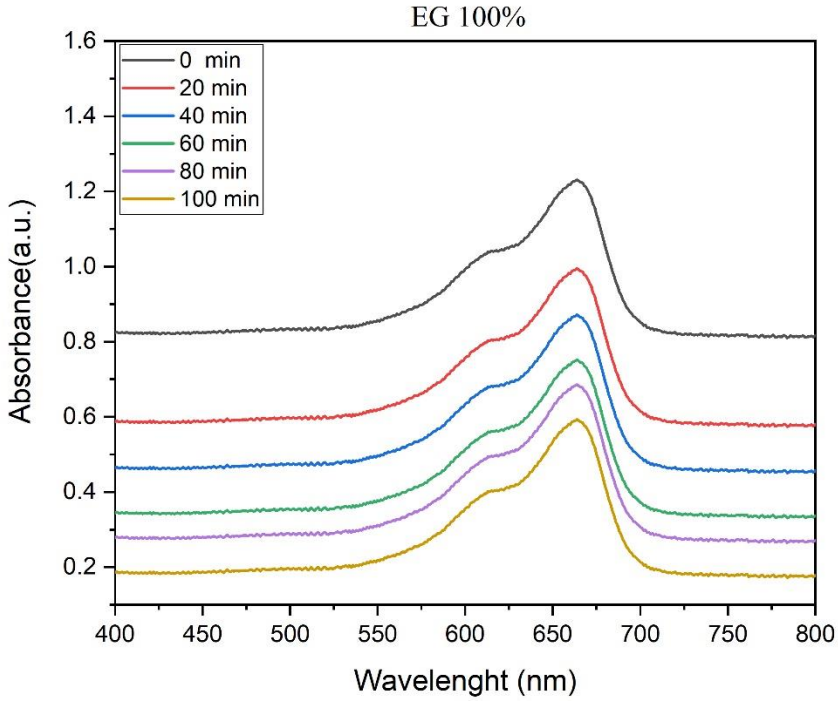

Figure (4.21) MB solution UV-Vis absorption spectra after photocatalysis for EG100% sample with different reaction times.

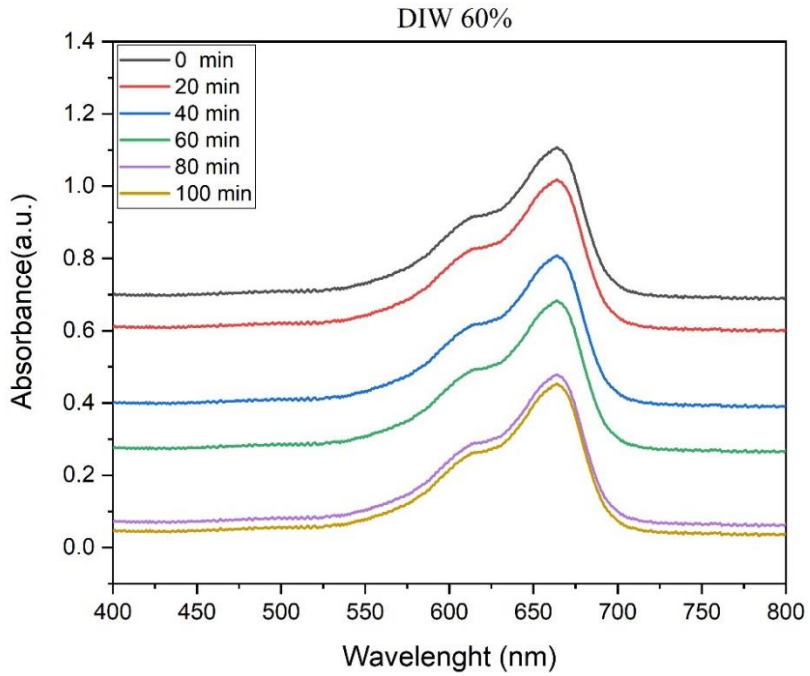

Figure (4.22) MB solution UV-Vis absorption spectra after photocatalysis for DIW60% sample with different reaction times.

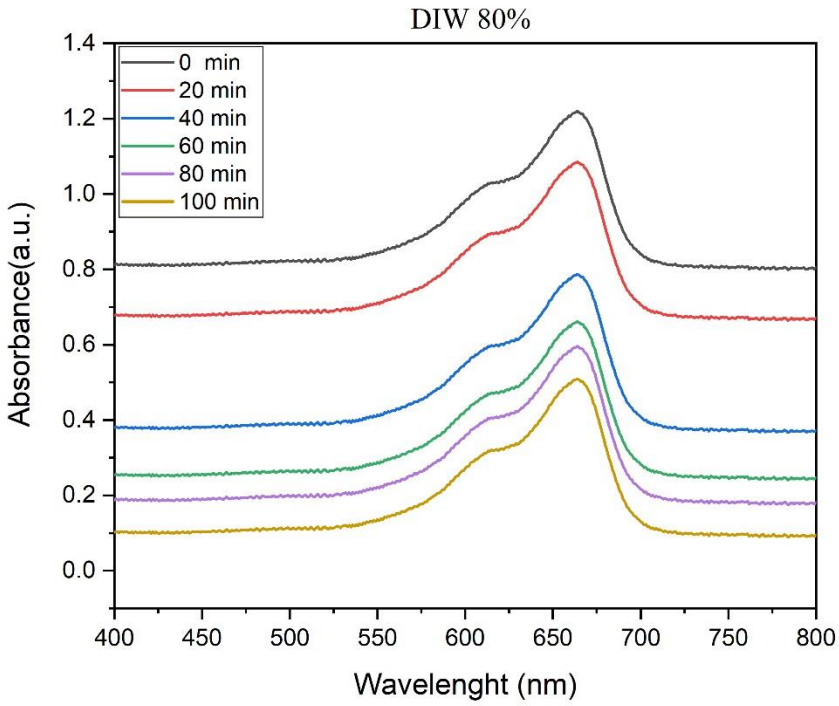

Figure (4.23) MB solution UV-Vis absorption spectra after photocatalysis for DIW80% sample with different reaction times.

The photodegradation rate of aqueous MB solution using TiO_2 nanoparticles samples as a function of the irradiation time under UV irradiation was displayed in figure (4.24). As shown in the figure, the evolution of the normalization of organic contaminated MB was confirmed by plotting the dye concentration ratio (C_t/C_o) as a function of the time irradiation (t). The blank run (without UV irradiation) of the samples was about (1.96%) of MB degradation after 100 min, which was a constringent reduction. The blank run showed that the degradation of MB could be ignored, as the MB solution cannot decompose without UV irradiation in the presence of the catalyst.

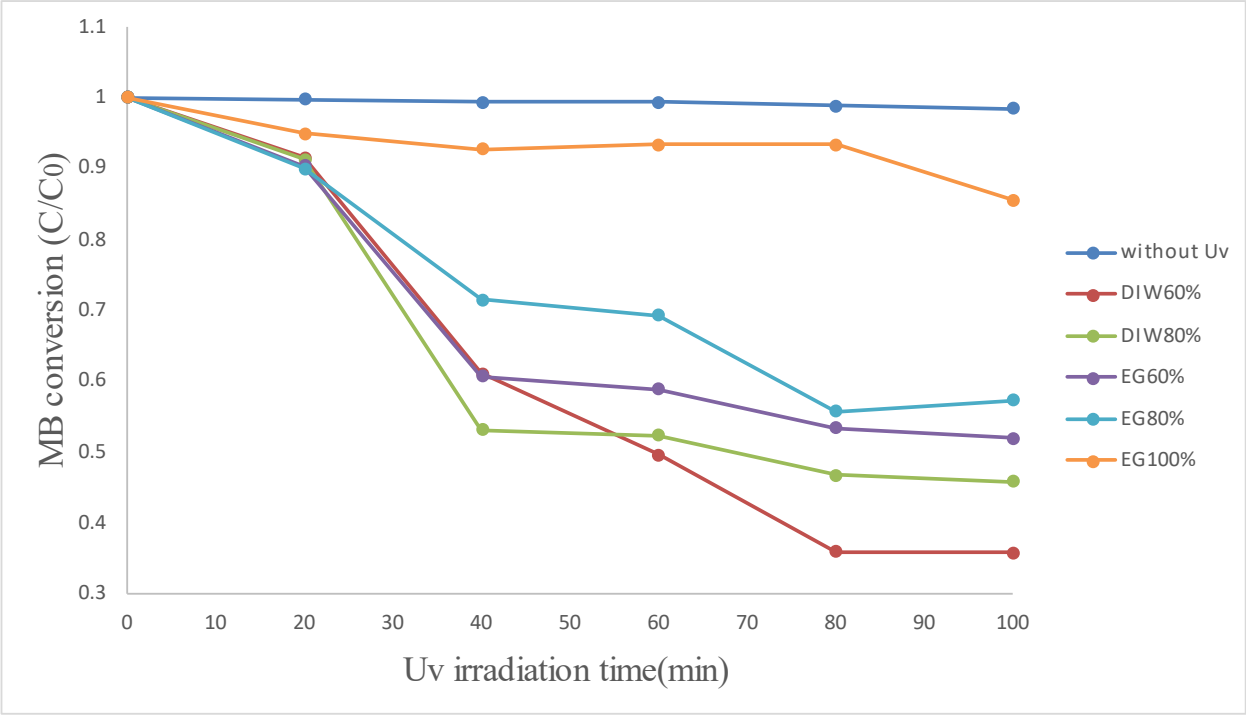

Figure (4.24) Photocatalytic decolorization behavior of MB using prepared TiO_2 nanoparticles samples.

Therefore, all of the TiO_2 nanoparticles samples showed more MB degradation under UV irradiation but with different photodegradation rates. The degradation ratio of the MB from the solution for the samples (DIW60%, DIW80%, EG60%, EG80% and EG100%) was found to be (64.33%, 54.24%, 48.12%, 42.78% and 23.51%) respectively.

The minimum performance of MB removal was achieved by the EG100% sample due to it having the lowest surface area. While the maximum performance of MB removal was achieved by the DIW60% sample because it had the highest surface area. It was concluded that the increase in the surface area of the TiO_2 catalyst leads to an increase in the interaction rate with the dye molecules, which was confirmed via the BET measurements. Table (4.7) illustrates the percent of obtained degradation after the photocatalytic reaction with the prepared TiO_2 nanoparticle samples.

Table (4.7) The percent of obtained degradation after the photocatalytic reaction with the prepared TiO_2 nanoparticles samples.

Sample	**Degradation Percent MB (%)**
DIW60%	64.22
DIW80%	54.24
EG60%	48.12
EG80%	42.78
EG100%	23.51

Moreover, the EG samples have a one-dimensional structure (nanorods) which enables better contact with MB in an aqueous solution, yielding more benefits for the process of photodegradation. TiO_2 with a 1D structure has exhibited a faster process of generating electron-hole pairs and a lower recombination rate. While the DIW samples have a higher interaction rate with the dye molecules due to the wider and broader distribution of space among particles in the spherical structure (as shown in the FESEM images).

The determined data for the pseudo-first-order kinetics constant (k) of TiO_2 samples as catalysts calcined at 400 ^oC in a concentration of 10 ppm of MB was achieved by plotting of ln (C_t/C_o) versus the irradiation time, which appears a straight line as shown

in figure (4.25). The slope equals first-order kinetics rate constant (k) for different photocatalysts, which has been utilized as a comparison parameter of the photodegradation because it depends on the surface area of the prepared samples [86].

From the figure, the MB degradation rate by TiO_2 nanoparticle samples appeared with different values under UV irradiation. The kinetic rate constant (k) of the samples (DIW60%, DIW80%, EG60%, EG80% and EG100%) are (10.3×10^{-3}, 7.81×10^{-3}, 6.51×10^{-3}, 5.58×10^{-3} and 2.68×10^{-3}) min^{-1} respectively. The best catalyst was the DIW60% sample with kinetics rate constant approximate about (10.3×10^{-3}) min^{-1}, due to its large surface area and it has many effective absorption sites. Therefore, MB was absorbed by the sample prior to being in the decomposition process, so the rate of reaction was faster than other samples studied.

Therefore, the sample EG100% has a lower performance for MB dye photodegradation compared with the other prepared TiO_2 nanoparticle samples. Table (4.8) summarizes the first-order rate constant (k) of the prepared TiO_2 nanoparticle samples.

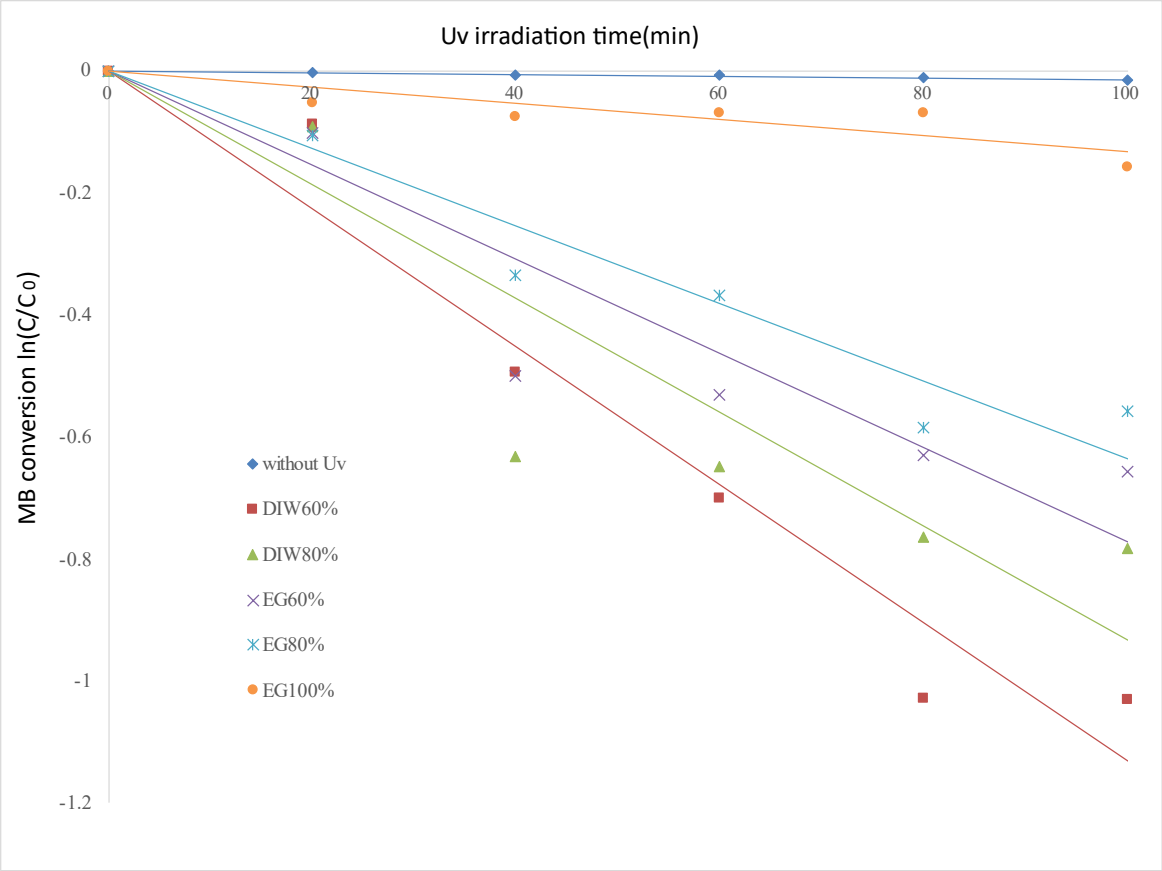

Figure (4.25) The first-order-kinetics of photocatalytic degradation of MB solution using the prepared TiO_2 nanoparticles samples.

Table (4.8) First-order kinetic constants (k) for photocatalytic degradation using the prepared TiO_2 nanoparticles after 100 min of UV irradiation.

Sample	First-order kinetic constant (k) (min^{-1}) $\times 10^{-3}$
DIW60%	10.3
DIW80%	7.81
EG60%	6.51
EG80%	5.58
EG100%	2.68

4.7 Conclusion

In this work, anatase titanium dioxide (TiO_2) nanoparticles were synthesized successfully as photocatalyst via microwave method with two different solvents, Ethylene Glycol (EG) and Deionized Water (DIW), at three different selected powers and annealed at 400 ºC for 1h for the photodegradation of organic pollutants Methylene Blue (MB). This work showed that the microwave technique is simple, rapid, convenient, and important for the synthesis of the TiO_2 nanoparticles due to the advantages of its heating mechanism over regular heating. According to the previous dissection and analysis, the following conclusions can be summarized:

1. The XRD analysis deduced that the TiO_2 nanoparticles synthesized in this work exist in the anatase TiO_2 phase. The diffraction peaks of the prepared samples detect a sharp domain (101) peak at about $2\theta=25.28^{o}$. The X-ray patterns also showed that there are no peaks of other materials, indicating the samples were prepared with a high degree of purity.
2. The FESEM images showed uniform rod-like shapes with distinct sizes for the EG samples and non-uniform spherical shapes for the DIW samples. These results revealed that the use of different solvents affected the morphology of the nanoparticles. TiO_2 nanorods became longer, distinguishable, and much thinner at the higher powers. The increase in power caused an increase in the size of the nanoparticles, which means that there is a proportional relationship between these two.
3. The EDX results revealed that the spectra consisted of Titanium (Ti) and Oxygen (O) peaks with high intensity indicating the successful synthesis of pure TiO_2 nanoparticles. The EG60% sample had the highest amount of Ti and the lowest amount of O elements, which indicated more produced TiO_2 nanoparticles.

4. The BET analysis revealed that the samples showed a type IV isotherm. It can be noticed that the DIW samples have a higher surface area and a higher pore size than the EG samples. The DIW60% sample had the highest surface area and pore size than the other samples.
5. The FT-IR results reveal that the IR spectra of the prepared samples show a broad absorption peak at (721 – 748) cm^{-1}. This peak reveals the growth of Ti-O stretching vibration in the anatase phase that denoted the strong absorbance of titanium dioxide TiO_2.
6. The photocatalytic activity tests indicated that the sample DIW60% showed a higher degradation rate of the MB than the other TiO_2 nanoparticle samples. The maximum performance of this sample reached 64.33% with the highest first-order kinetics constant about (10.3×10^{-3}) min^{-1}, due to the increase of the specific surface area of the catalyst and high porosity, which leads to an increased interaction rate with the dye molecules on the TiO_2 nanocatalyst surface.

4.8 Suggestions for the Future Research

Based on the finding in this study, many promising tasks can be suggested for the future research on the synthesis methods and enhancement of TiO_2 nanostructures photocatalytic activity, as follows:

1- Utilization of the microwave method can be achieved to synthesize other semiconductor metal oxide nanostructures such as ZnO, NiO, ZrO_2, etc.

2- Some metal and non-metal such as (Au, Pt, Fe, Cu. N and C) doped with TiO_2 nanostructure may be achieved using this method, due to the wide area of applications for these nanomaterial structures.

3- The effect of other experimental parameters in photocatalyst activity such as the concentration of precursor, the temperature of calcination, PH solution, light intencity and selected wavelength, may be extensively studied.

4- The methylene blue (MB) degradation using the prepared nano-crystal structures was studied and a very promising finding was obtained under the ultraviolet (UV) irradiation. Therefore, it is important to examine various kinds of dyes such as Rhodamine B dye, carmine dye, methyl red dye, congo red and methyl orange, in order to study the photocatalytic activity of the prepared nano-catalysts.

5- More time should be concentrated on the applications and the optimization of doping TiO_2 with other nanomaterials. It is interesting to employ these nanomaterials in carbon dioxide (CO_2) reduction in the atmosphere, hydrogen generation, the gas sensing and solar cells, due to wide range applications of TiO_2.

References

[1] Dąbrowski, A., P. Podkościelny, Z. Hubicki, and M. Barczak, *Adsorption of phenolic compounds by activated carbon—a critical review.* Chemosphere, 2005. **58**(8): pp 1049-1070.

[2] Dvorak, B.I. and S. Skipton, *G08-1489 Drinking Water Treatment: Activated Carbon Filtration.* 2008.

[3] Pfeifer, V., P. Erhart, S. Li, K. Rachut, J. Morasch, J. Brötz, P. Reckers, T. Mayer, S. Rühle, and A. Zaban, *Energy band alignment between anatase and rutile TiO_2.* The Journal of Physical Chemistry Letters, 2013. **4**(23): pp 4182-4187.

[4] Gu, X.-N., M. Ye, X.-L. Wu, L. Wei, Y. Hu, X.-G. Hou, X.-G. Liu, and A.-D. Liu, *Deposition of silver on titania films by electron beam irradiation.* Nuclear Instruments and Methods in Physics Research Section B: Beam Interactions with Materials and Atoms, 2006. **247**(2): pp 279-284.

[5] Kamat, P.V., *Photoinduced transformations in semiconductormetal nanocomposite assemblies.* Pure and Applied Chemistry, 2002. **74**(9): pp 1693-1706.

[6] Bazargan, M.H., M.M. Byranvand, and A.N. Kharat, *Preparation and characterization of low temperature sintering nanocrystalline TiO_2 prepared via the sol-gel method using titanium (IV) butoxide applicable to flexible dye sensitized solar cells.* International Journal of Materials Research, 2012. **103**(3): pp 347-351.

[7] Andersson, M., L. Österlund, S. Ljungstroem, and A. Palmqvist, *Preparation of nanosize anatase and rutile TiO_2 by hydrothermal treatment of microemulsions and their activity for photocatalytic wet oxidation of phenol.* The Journal of Physical Chemistry B, 2002. **106**(41): pp 10674-10679.

[8] Alosfur, F.K.M., N.J. Ridha, M.H.H. Jumali, and S. Radiman, *One-step formation of TiO_2 hollow spheres via a facile microwave-assisted process for photocatalytic activity.* Nanotechnology, 2018. **29**(14): pp 145707.

[9] Garzella, C., E. Comini, E. Tempesti, C. Frigeri, and G. Sberveglieri, *TiO_2 thin films by a novel sol–gel processing for gas sensor applications.* Sensors and Actuators B: Chemical, 2000. **68**(1-3): pp 189-196.

[10] Hornyak, G.L., J. Dutta, H.F. Tibbals, and A. Rao, *Introduction to nanoscience*. 2008: CRC press.

[11] Hulkoti, N.I. and T. Taranath, *Biosynthesis of nanoparticles using microbes—a review.* Colloids and Surfaces B: Biointerfaces, 2014. **121**: pp 474-483.

[12] Ventra, M., S. Evoy, and J.R. Heflin, *Introduction to nanoscale science and technology*. 2006: Springer Science & Business Media.

[13] Hu, E.L., S.M. Davis, R. Davis, and E. Scher, *Applications: catalysis by nanostructured materials*, in *Nanotechnology Research Directions for Societal Needs in 2020*. 2011, Springer. pp 445-466.

[14] Kuchibhatla, S.V., A. Karakoti, D. Bera, and S. Seal, *One dimensional nanostructured materials.* Progress in materials science, 2007. **52**(5): pp 699-913.

[15] Nikalje, A.P., *Nanotechnology and its applications in medicine.* Med chem, 2015. **5**(2): pp 081-089.

[16] Mohieldin, S., E. Zainudin, M. Paridah, and Z. Ainun. *Nanotechnology in pulp and paper industries: A Review*. in *Key Engineering Materials*. 2011. Trans Tech Publ.

[17] Sinha, N., N.M. Kulshreshtha, M. Dixit, I. Jadhav, D. Shrivastava, and P.S. Bisen, *Nanodentistry: novel approaches*, in *Nanostructures for Oral Medicine*. 2017, Elsevier. pp 751-776.

[18] Arole, V. and S. Munde, *Fabrication of nanomaterials by top-down and bottom-up approaches-an overview.* J. Mater. Sci, 2014. **1**: pp 89-93.

[19] Khan, H., *Synthesis, Characterization and Photocatalytic Activity of Titanium Dioxide (Pure and Doped) Photocatalyst for the Degradation of Aqueous Organic Pollutants*, in *Chemical Eng.* 2015, McGill University: Canada

[20] Kumar, A. and G. Pandey, *Different methods used for the synthesis of TiO2 based nanomaterials: A review.* American Journal of Nano Research and Applications, 2018. **6**(1): pp 1.

[21] Kwong, C.W., *Microwave Flow Synthesis of Nanostructured TiO_2*. 2010, Hong Kong University of Science and Technology: Hong Kong.

[22] Khataee, A. and G.A. Mansoori, *Nanostructured titanium dioxide materials: Properties, preparation and applications*. 2011: World scientific.

[23] Barnard, A., P. Zapol, and L. Curtiss, *Modeling the morphology and phase stability of TiO_2 nanocrystals in water.* Journal of Chemical Theory and Computation, 2005. **1**(1): pp 107-116.

[24] Farmer, J., *A comparison of conventional heating techniques and microwave irradiation for the desorption of lithium borohydride and lithium borohydride composites*. 2009, University of Birmingham.

[25] Carlucci, C., H. Xu, B.F. Scremin, C. Giannini, D. Altamura, E. Carlino, V. Videtta, F. Conciauro, G. Gigli, and G. Ciccarella, *Selective synthesis of TiO_2 nanocrystals with morphology control with the microwave-solvothermal method.* CrystEngComm, 2014. **16**(9): pp 1817-1824.

[26] Moura, K., J. Maul, A. Albuquerque, G. Casali, E. Longo, D. Keyson, A. Souza, J.R. Sambrano, and I. Santos, *TiO_2 synthesized by microwave assisted solvothermal method: Experimental and theoretical evaluation.* Journal of Solid State Chemistry, 2014. **210**(1): pp 171-177.

[27] Xu, H., C. Carlucci, B.F. Scremin, C. Giannini, T. Sibillano, A. Scrascia, A.L. Capodilupo, G. Gigli, and G. Ciccarella, *Synthesis of ultrafine anatase titanium dioxide (TiO_2) nanocrystals by the microwave-solvothermal method.* Journal of Nanoengineering and Nanomanufacturing, 2014. **4**(1): pp 28-32.

[28] Lu, C.-W., Y. Cao, H. Li, C. Webb, and W.-P. Pan, *Synthesis of TiO_2 based on hydrothermal methods using elevated pressures and microwave conditions.* Journal of Thermal Analysis and Calorimetry, 2014. **116**(3): pp 1241-1248.

[29] Filippo, E., C. Carlucci, A.L. Capodilupo, P. Perulli, F. Conciauro, G.A. Corrente, G. Gigli, and G. Ciccarella, *Enhanced photocatalytic activity of pure anatase TiO_2 and Pt-TiO_2 nanoparticles synthesized by green microwave assisted route.* Materials Research, 2015. **18**(3): pp 473-481.

[30] Mohadesi, A. and M. Ranjbar, *Synthesis and characterization of TiO_2 nanoparticles by microwave method and investigation its photovoltaic property.* Journal of Materials Science: Materials in Electronics, 2016. **27**(1): pp 862-866.

[31] Ranjan, S., N. Dasgupta, B. Rajendran, G.S. Avadhani, C. Ramalingam, and A. Kumar, *Microwave-irradiation-assisted hybrid chemical approach for titanium dioxide nanoparticle synthesis: microbial and cytotoxicological evaluation.* Environmental Science and Pollution Research, 2016. **23**(12): pp 12287-12302.

[32] Joshi, D.N. and R.A. Prasath, *Low temperature rapid synthesis of direct mesoporous anatase TiO2nano-aggregates and its application in dye-sensitized solar cell.* Materials Today: Proceedings, 2016. **3**(6): pp 2413-2421.

[33] Su, C.-H., C.-C. Hu, Y.-C.C. Sun, and Y.-C. Hsiao, *Highly active and thermo-stable anatase TiO_2 photocatalysts synthesized by a microwave-assisted hydrothermal method.* Journal of the Taiwan Institute of Chemical Engineers, 2016. **59**: pp 229-236.

[34] Cabello, G., R.A. Davoglio, and E.C. Pereira, *Microwave-assisted synthesis of anatase-TiO_2 nanoparticles with catalytic activity in oxygen reduction.* Journal of Electroanalytical Chemistry, 2017. **794**: pp 36-42.

[35] Santhosh, N., R. Govindaraj, M.S. Pandian, and P. Ramasamy. *Facile synthesis of mesoporous TiO_2 nanospheres by microwave-assisted hydrothermal method and its applications in dye sensitized solar cells*. in *AIP Conference Proceedings*. 2017. AIP Publishing LLC.

[36] Bregadiolli, B.A., S.L. Fernandes, and C.F.d.O. Graeff, *Easy and fast preparation of TiO_2-based nanostructures using microwave assisted hydrothermal synthesis.* Materials Research, 2017. **20**(4): pp 912-919.

[37] Anitha, R., E. Kumar, and S. Vijayalakshmi, *Prepartion and characterization of TiO_2 nano particles via Microwave assisted Solvothermal method.*

[38] Andrade-Guel, M., L. Díaz-Jiménez, D. Cortés-Hernández, C. Cabello-Alvarado, C. Ávila-Orta, P. Bartolo-Pérez, and P. Gamero-Melo, *Microwave assisted sol–gel synthesis of titanium dioxide using hydrochloric and acetic acid as catalysts.* Boletín de la Sociedad Española de Cerámica y Vidrio, 2019. **58**(4): pp 171-177.

[39] Vinodhini, J., J. Mayandi, R. Atchudan, P. Jayabal, V. Sasirekha, and J.M. Pearce, *Effect of microwave power irradiation on TiO_2 nano-structures and binder free paste screen printed dye sensitized solar cells.* Ceramics International, 2019. **45**(4): pp 4667-4673.

[40] Almashhori, K., T.T. Ali, A. Saeed, R. Alwafi, M. Aly, and F.E. Al-Hazmi, *Antibacterial and photocatalytic activities of controllable (anatase/rutile) mixed phase TiO_2 nanophotocatalysts synthesized via a microwave-assisted sol–gel method.* New Journal of Chemistry, 2020. **44**(2): pp 562-570.

[41] Ayyaz, M., M. Naz, M. Marriam, M. Akram, Z. Hussain, S. Shukrullah, and I. Toqeer. *Microwave plasma assisted sol-gel technique for synthesis of TiO_2 nanoparticles.* in *IOP Conference Series: Materials Science and Engineering*. 2020. IOP Publishing.

[42] Rezvani Nikabadi, H. and S. Khosroababdi, *Synthesis of TiO_2 nanorods with a microwave assisted solvothermal method and their application as dye-sensitized solar cells.* Journal of Nanoanalysis, 2019.

[43] Imoisili, P.E., T.-C. Jen, and B. Safaei, *Microwave-assisted sol–gel synthesis of TiO2-mixed metal oxide nanocatalyst for degradation of organic pollutant.* Nanotechnology Reviews, 2021. **10**(1): pp 126-136.

[44] Ollis, D., E. Pelizzetti, and N. Serpone, *Photocatalysis: fundamentals and applications.* Serpone and E. Pellizzetti (eds.) John Wiley and Sons, New York, 1989. **603**.

[45] Braslavsky, S.E., *Glossary of terms used in photochemistry, (IUPAC Recommendations 2006).* Pure and Applied Chemistry, 2007. **79**(3): pp 293-465.

[46] Masel, R.I., *Chemical kinetics and catalysis*. Vol. 10. 2001: Wiley-Interscience New York.

[47] JINKAI, Z., *Modified Titanium Dioxide (TiO_2) photocatalysts for the degradation of organic pollutants in wastewater.* 2007.

[48] Mills, A. and S. Le Hunte, *An overview of semiconductor photocatalysis.* Journal of photochemistry and photobiology A: Chemistry, 1997. **108**(1): pp 1-35.

[49] Yang, P., D. Zhao, D.I. Margolese, B.F. Chmelka, and G.D. Stucky, *Generalized syntheses of large-pore mesoporous metal oxides with semicrystalline frameworks.* Nature, 1998. **396**(6707): pp 152-155.

[50] Gaya, U.I. and A.H. Abdullah, *Heterogeneous photocatalytic degradation of organic contaminants over titanium dioxide: a review of fundamentals, progress and problems.* Journal of photochemistry and photobiology C: Photochemistry reviews, 2008. **9**(1): pp 1-12.

[51] Wang, X. and R.A. Caruso, *Enhancing photocatalytic activity of titania materials by using porous structures and the addition of gold nanoparticles.* Journal of Materials Chemistry, 2011. **21**(1): pp 20-28.

[52] Maschmeyer, T., F. Rey, G. Sankar, and J.M. Thomas, *Heterogeneous catalysts obtained by grafting metallocene complexes onto mesoporous silica.* Nature, 1995. **378**(6553): pp 159-162.

[53] Khataee, A. and M.B. Kasiri, *Photocatalytic degradation of organic dyes in the presence of nanostructured titanium dioxide: Influence of the chemical structure of dyes.* Journal of Molecular Catalysis A: Chemical, 2010. **328**(1-2): pp 8-26.

[54] Mukhlish, M.B., F. Najnin, M.M. Rahman, and M. Uddin, *Photocatalytic degradation of different dyes using TiO_2 with high surface area: a kinetic study.* Journal of Scientific Research, 2013. **5**(2): pp 301-314.

[55] Diebold, U., *The surface science of titanium dioxide.* Surface science reports, 2003. **48**(5-8): pp 53-229.

[56] Hoffmann, M.R., S.T. Martin, W. Choi, and D.W. Bahnemann, *Environmental applications of semiconductor photocatalysis.* Chemical reviews, 1995. **95**(1): pp 69-96.

[57] Nosaka, Y., T. Daimon, A.Y. Nosaka, and Y. Murakami, *Singlet oxygen formation in photocatalytic TiO_2 aqueous suspension.* Physical Chemistry Chemical Physics, 2004. **6**(11): pp 2917-2918.

[58] Chen, Y., Z. Sun, Y. Yang, and Q. Ke, *Heterogeneous photocatalytic oxidation of polyvinyl alcohol in water.* Journal of Photochemistry and Photobiology A: Chemistry, 2001. **142**(1): pp 85-89.

[59] Arai, Y., *Chemistry of powder production*. Vol. 6. 1996: Springer Science & Business Media.

[60] C. Mwolfe, N.H.a.G.S., *Physical properties of Semiconductor*. 1989, New York: prentice Hall.

[61] Touloukian, Y., R. Kirby, E. Taylor, and T. Lee, *Thermophysical Properties of Matter-the TPRC Data Series. Volume 13. Thermal Expansion-Nonmetallic Solids*. 1977, THERMOPHYSICAL AND ELECTRONIC PROPERTIES INFORMATION ANALYSIS CENTER LAFAYETTE IN.

[62] Webb, P. and C. Orr, *Surface area and pore structure by gas adsorption.* Analytical methods in fine particle technology, 1997: pp 54-153.

[63] Schumacher, K., M. Grün, and K. Unger, *Novel synthesis of spherical MCM-48.* Microporous and Mesoporous Materials, 1999. **27**(2-3): pp 201-206.

[64] Storck, S., H. Bretinger, and W.F. Maier, *Characterization of micro-and mesoporous solids by physisorption methods and pore-size analysis.* Applied Catalysis A: General, 1998. **174**(1-2): pp 137-146.

[65] Goldstein, J., *Practical scanning electron microscopy: electron and ion microprobe analysis*. Springer Science & Business Media. 2012.

[66] Zhou, W. and Z.L. Wang, *Scanning microscopy for nanotechnology: techniques and applications*. Springer science & business media. 2007.

[67] Baron, A.S., *Synthesis and Characterization of methyl ammonium lead tri halide Perovskite Compounds and their Applications in Photonic Devices. University of Basrah*. 2019, University of Basrah.

[68] Hubbard, A.T., *The Handbook of surface imaging and visualization*. 1995: CRC press.

[69] Potts, P.J., J. Bowles, S.J. Reed, and R. Cave, *Microprobe techniques in the Earth Sciences*. Vol. 6. 1995: Springer Science & Business Media.

[70] Silverstein, R.M. and G.C. Bassler, *Spectrometric identification of organic compounds.* Journal of Chemical Education, 1962. **39**(11): p. 546.

[71] Perkampus, H.-H., *Analytical Applications of UV-VIS Spectroscopy*, in *UV-VIS Spectroscopy and Its Applications*. 1992, Springer. pp 26-80.

[72] Sellappan, R., *Mechanisms of enhanced activity of model TiO_2/carbon and TiO_2/metal nanocomposite photocatalysts*. Chalmers University of Technology. 2013.

[73] Yu, J., G. Wang, B. Cheng, and M. Zhou, *Effects of hydrothermal temperature and time on the photocatalytic activity and microstructures of bimodal mesoporous TiO_2 powders.* Applied Catalysis B: Environmental, 2007. **69**(3-4): pp 171-180.

[74] Wagner, M., K. Köhler, L. Djakovitch, S. Weinkauf, V. Hagen, and M. Muhler, *Heck reactions catalyzed by oxide-supported palladium–structure–activity relationships.* Topics in Catalysis, 2000. **13**(3): pp 319-326.

[75] Yu, J. and L. Shi, *One-pot hydrothermal synthesis and enhanced photocatalytic activity of trifluoroacetic acid modified TiO_2 hollow microspheres.* Journal of Molecular Catalysis A: Chemical, 2010. **326**(1-2): pp 8-14.

[76] Sing, K.S., *Reporting physisorption data for gas/solid systems with special reference to the determination of surface area and porosity (Recommendations 1984).* Pure and applied chemistry, 1985. **57**(4): pp 603-619.

[77] Huang, C.-H., Y.-T. Yang, and R.-A. Doong, *Microwave-assisted hydrothermal synthesis of mesoporous anatase TiO_2 via sol–gel process for dye-sensitized solar cells.* Microporous and Mesoporous Materials, 2011. **142**(2-3): pp 473-480.

[78] Lowell, S. and J.E. Shields, *Powder surface area and porosity*. Vol. 2. 2013: Springer Science & Business Media.

[79] Lee, H.-B., M.-S. Choi, Y.-H. Kye, M.-Y. An, and I.-M. Lee, *Control of particle characteristics in the preparation of TiO_2 nano particles assisted by microwave.* Bulletin of the Korean Chemical Society, 2012. **33**(5): pp 1699-1702.

[80] Brantley, S.L. and N.P. Mellott, *Surface area and porosity of primary silicate minerals.* American Mineralogist, 2000. **85**(11-12): pp 1767-1783.

[81] Praveen, P., G. Viruthagiri, S. Mugundan, and N. Shanmugam, *Structural, optical and morphological analyses of pristine titanium di-oxide nanoparticles–Synthesized via sol–gel route.* Spectrochimica Acta Part A: Molecular and Biomolecular Spectroscopy, 2014. **117**: pp 622-629.

[82] Fathy, M. and H. Hamad, *Influence of calcination temperatures on the formation of anatase TiO_2 nano rods with a polyol-mediated solvothermal method.* RSC advances, 2016. **6**(9): pp 7310-7316.

[83] Carlucci, C., B.F. Scremin, T. Sibillano, C. Giannini, E. Filippo, P. Perulli, A.L. Capodilupo, G.A. Corrente, and G. Ciccarella, *Microwave-assisted synthesis of boron-modified TiO_2 nanocrystals.* Inorganics, 2014. **2**(2): pp 264-277.

[84] Nag, M., P. Basak, and S.V. Manorama, *Low-temperature hydrothermal synthesis of phase-pure rutile titania nanocrystals: Time temperature tuning of morphology and photocatalytic activity.* Materials Research Bulletin, 2007. **42**(9): pp 1691-1704.

[85] Yogi, C., K. Kojima, N. Wada, H. Tokumoto, T. Takai, T. Mizoguchi, and H. Tamiaki, *Photocatalytic degradation of methylene blue by TiO_2 film and Au particles-TiO_2 composite film.* Thin Solid Films, 2008. **516**(17): pp 5881-5884.

[86] Konstantinou, I.K. and T.A. Albanis, *Photocatalytic transformation of pesticides in aqueous titanium dioxide suspensions using artificial and solar light: intermediates and degradation pathways.* Applied Catalysis B: Environmental, 2003. **42**(4): pp 319-335.

الخلاصة

في هذه الدراسة، تم تحضير ثنائي أوكسيد التيتانيوم (TiO_2) باستخدام طريقة الميكروويف كطريقة سريعة وغير مكلفة وفعالة. تم استخدام مذيبين مختلفين من أجل دراسة تأثيرطاقة المايكروويف و المذيب على عملية التّشكل وحجم الجسيمات والمساحة السطحية للعينات المحضرة. المذيب الأول كان ايثيلين كلايكول (EG 99.8%)، والآخر عبارة عن ماء منزوع الأيونات (DIW)، بينما تم استخدام أوكسيد التيتانيوم الأيزوبروبوكسيد (TTIP) $Ti[OCH(CH3)_2]_4$ كمادة اساس لـ (TiO_2) . تم استخدام فرن ميكروويف تجاري بثلاث مستويات مختلفة من الطاقة مع مدة تحضير بلغت 5 دقائق لكل عينة. تم تلدين العينات المحضرة عند 400 درجة مئوية لمدة ساعة واحدة.

في هذا العمل، تم استخدام تقنيات متنوعة لدراسة بُنية ومورفولوجيا العينات المحضرة، حيود الاشعة السينية (XRD)، مساحة السطح المحددة بتقنية (BET)، المجهر الالكتروني الماسح مع التحليل الطيفي للأشعة السينية المشتتة للطاقة (FESEM-EDX) و مطياف الاشعة تحت الحمراء (FTIR). من خلال النتائج العملية، أوضحت نتائج (XRD) أن العينات المحضرة كانت ثنائي أوكسيد تيتانيوم نقياً في طور (anatase)، وهو ما أكدته نتائج (EDX) ايضاً. تم حساب المساحة السطحية لـقضبان (TiO_2) النانوية باستخدام تحليل (BET)، والذي أوضح أن العينات لها مساحة سطحية كبيرة و مسامية عالية (المساحة السطحية لعينات DIW كانت أعلى من عينات EG). أظهرت نتائج (FESEM) أن عينات (TiO_2) المحضرة كانت تشبه القضبان النانوية عند استخدام (EG) كمذيب. في المقابل، تم الحصول على جسيمات نانوية ذات شكل كروي على هيئة تكتلات عند استخدام (DIW) كمذيب. بينما أدت الزيادة في الطاقة إلى زيادة حجم الجسيمات النانوية. أظهرت قياسات (FTIR) أنماط الاهتزاز في طيف العينات، مما يشير إلى تكوين O-Ti-O.

تمت دراسة أداء العينات المحضرة لمعالجة المياه باستخدام آلية التحلل الضوئي المعياري. تم استخدام الميثيلين الأزرق (MB) بتركيز (10 ppm) في الماء منزوع الأيونات كنظام ملوث. أُجريت جميع التجارب تحت الأشعة فوق البنفسجية لمدة (120 دقيقة) من وقت التعرض. لوحظت أعلى نسبة إزالة للميثيلين الأزرق من المحلول في عينة ٪60 DIW ، والتي وصلت إلى حوالي ٪64.22 تحت إشعاع UV خلال فترة التعرض. يأتي ذلك بسبب الزيادة في مساحة سطح العينة.

جمهورية العراق
وزارة التعليم العالي
و البحث العلمي
جامعة كربلاء
كلية العلوم
قسم الفيزياء

تحضير و توصيف جسيمات ثنائي أوكسيد التيتانيوم النانوية بإستخدام المايكروويف وتطبيقها في معالجة المياه

رسالة
مقدمة الى قسم الفيزياء في جامعة كربلاء وهي جزء
من متطلبات نيل شهادة الماجستير في علوم الفيزياء

تقدم بها

رضا صلاح محمد
جلوخان

إشراف

أ.م.د. فراس كامل محمد العصفور
أ.د. أحمد محمود عبد اللطيف

2021 م **1442 هـ**